


Review

# A Review on the Fabrication and Characterization of Titania Nanotubes Obtained via Electrochemical Anodization

Syeda Ammara Batool <sup>1</sup>, Muhammad Salman Maqbool <sup>1</sup>, Muhammad Awais Javed <sup>2</sup>, Akbar Niaz <sup>3</sup>  
and Muhammad Atiq Ur Rehman <sup>1,\*</sup>

<sup>1</sup> Department of Materials Science and Engineering, Institute of Space Technology Islamabad, Islamabad Highway, Islamabad 44000, Pakistan

<sup>2</sup> School of Science, Computing and Engineering Technologies, Swinburne University of Technology, Hawthorn 3122, Australia

<sup>3</sup> Department of Mechanical Engineering, King Faisal University, Al Hufuf 31982, Saudi Arabia

\* Correspondence: atique1.1@hotmail.com

**Abstract:** Recently, titania nanotubes (TNTs) have been extensively studied because both their functional properties and highly controllable morphology make them important building blocks for understanding nanoscale phenomena and realizing nanoscale devices. Compared with sol-gel and template-assisted methods, electrochemical anodization is a simple, cost-effective, and low-temperature technique offering additional advantages such as straightforward processing and ease of scale-up. This review focuses on the process modalities and underlying mechanism of electrochemical anodization to achieve a different set of TNTs for a variety of applications. Finally, important applications of TNTs are highlighted including biomedical devices, water purification, and solar cells.

**Keywords:** titania; nanotubes; anodization; biomedical; solar cells; water purification



**Citation:** Batool, S.A.; Salman Maqbool, M.; Javed, M.A.; Niaz, A.; Rehman, M.A.U. A Review on the Fabrication and Characterization of Titania Nanotubes Obtained via Electrochemical Anodization. *Surfaces* **2022**, *5*, 456–480. <https://doi.org/10.3390/surfaces5040033>

Academic Editor: Gaetano Granozzi

Received: 27 September 2022

Accepted: 7 November 2022

Published: 9 November 2022

**Publisher's Note:** MDPI stays neutral with regard to jurisdictional claims in published maps and institutional affiliations.



**Copyright:** © 2022 by the authors. Licensee MDPI, Basel, Switzerland. This article is an open access article distributed under the terms and conditions of the Creative Commons Attribution (CC BY) license (<https://creativecommons.org/licenses/by/4.0/>).

## 1. Introduction

Nanomaterials have attracted many scientists and engineers from a variety of fields to a common ground during the last three decades [1]. Research based on the fabrication, characterization, and applications of nanomaterials (material length scales of less than 100 nm) has revolutionized the field of science and technology due to the versatile electric, mechanical, and optical properties of nanomaterials. This field was coined the name “nanotechnology” by Norio Taniguchi in 1974 [2,3].

Nanotubular materials exhibit unique hierarchical architecture, excellent electrical and mechanical properties, and high specific surface area [4]. First, it provides a significant increase in the surface area to volume ratio and change in the size of a nanoparticle taking it into a sphere where the quantum effect predominates [5]. This increase in the surface area to volume ratio leads to the increased dominance of the behavior of an atom on the surface of particles [6]. The high surface area plays a crucial role in the performance of catalysis and energy storage applications, i.e., batteries, supercapacitors, and piezoelectric, triboelectric, photovoltaic, and catalytic materials [7,8]. Nanoscale materials are used to develop new technologies to make full use of abundant “green” energy sources. This all becomes possible because of the large surface area of the nanomaterials [9]. A certain decrease in the size of particles leads them to exhibit quantum mechanical behavior. It is a well-known fact that nanoparticles have dimensions below the critical wavelength of light, which makes them transparent. This property is crucial for applications in cosmetics, coating, and packaging [10].

Nanostructured transition metal oxides, particularly one-dimensional nanorods, nanowires, and nanotubes, have been widely researched due to their widespread applications [11]. A wide variety of nanostructures can be synthesized with high control of

dimension and morphology by the use of various techniques. Electrochemical synthesis is the most promising method to obtain a nanostructure with great accuracy [12].

Titanium has gained much attention over the past few years because of its high corrosion resistance, low density, and strong durability. A passive oxide film is formed, which makes it particularly resistant to corrosion in oxidizing solutions. This passive layer is the compound of titanium and oxygen having the formula  $\text{TiO}_2$ . Different types of  $\text{TiO}_2$  nanostructures can be formed, and each type has its own pros and cons. Shen et al. [8] studied various  $\text{TiO}_2$  nanostructures for photoelectrochemistry (PEC) applications, including 1-D (nanowires, nanotubes, and nanorods), 2-D (nanobelt, nanosheet, and nanoribbon), 3-D (meso/nanoporous and branched nanostructures), and the crystal-facet-tailored  $\text{TiO}_2$  nanostructures. As compared to other morphologies,  $\text{TiO}_2$  nanotubes (TNTs) had large surface areas and extended length in one direction due to which they showed better performance for PEC  $\text{CO}_2$  reduction. This characteristic also makes them suitable for holding different moieties on their surface for other applications as well [13].

TNTs are important functional materials owing to their unique electronic properties, chemical stability, photo-corrosion resistance, and biocompatibility [5,13,14]. Compared with other metallic oxides,  $\text{TiO}_2$  provides biocompatibility in terms of low ion release and excellent corrosion resistance [13–15]. The biocompatibility of titanium is a result of the presence of a surface native oxide layer (passive film) of 2–5 nm thickness, which is naturally formed as titanium is exposed to air [15].

For nearly three decades now, titania nanotubes (TNTs) have attracted widespread scientific and technological interest. Along with a high aspect ratio and surface area, high-quality TNTs exhibit remarkable mechanical properties, environmental photocatalysis, and photo-splitting of water, which makes them attractive materials for a wide range of applications [16–18]. For example, they are used in gas-sensing devices, sensitized solar cells, photoelectrochemical cells, biomedical devices, the coatings industry, and sunscreens [19–21]. TNTs can significantly reduce the elastic modulus of Ti. Thus, minimizing the chances of stress shielding, which can arise due to the difference in the elastic moduli of bone and the implant. Moreover, TNTs can enhance the mineralization tendency and improve the interaction with the osteoblast cell by virtue of their surface topography, i.e., wettability and surface roughness [22]. In addition, TNTs can also be utilized for designing drug delivery systems [16,21,23,24]. Mansoorianfar et al. [25] fabricated tunable TNTs at different voltages for loading vancomycin to induce an antibacterial effect on a Ti64-based implant as shown in Figure 1. TNTs also have wide applications in the energy sector. The rapid depletion of fossil fuels and  $\text{CO}_2$  emissions has diverted the research focus to clean and renewable energy sources. Solar energy is the biggest and cheapest source of energy to date. The photovoltaic effect converts the photons into electricity, and around 20 GW of energy was produced in 2020 in the USA, benefitting 17 million households [26].

Self-organized TNTs can be produced by anodization, sol-gel, hydrothermal, and vapor deposition methods. Electrochemical anodization is a simple and low-cost method, which can synthesize TNTs with ordered nanostructures for a variety of applications [17,18]. However, one of the challenges to synthesize TNTs via electrochemical anodization is the chemical stability of Ti (only a few chemical compounds such as HF and  $\text{H}_2\text{O}_2$  can chemically dissolve Ti). Different process parameters affect the configuration, shape, and dimensions of TNTs [27,28]. TNTs' growth is directly related to anodization time, voltage, and fluoride ion concentration in the electrolyte [29]. TNTs of desired diameters or dimensions can be obtained by varying the applied potential or concentration of electrolytes. The length of nanotubes can be increased or decreased by varying the pH of the electrolyte and/or anodizing time [30,31]. The optimization of the anodizing conditions is very crucial to obtain TNTs with specific properties. The pre-surface condition, voltage ramp, nature of the electrolyte, and fluoride ion concentration are major concerns [27,32]. Moreover, in addition to controlling the dimensions and surface characteristics of TNTs for suggested applications, the mechanical stability of TNTs is also important for performance and long-term functions [23,31]. Furthermore, the crystallinity of the synthesized TNTs determines

their performance in photovoltaic and biomedical applications [33]. It is important to choose the appropriate heat treatment parameters for the synthesized TNTs in relation to the final applications [32].

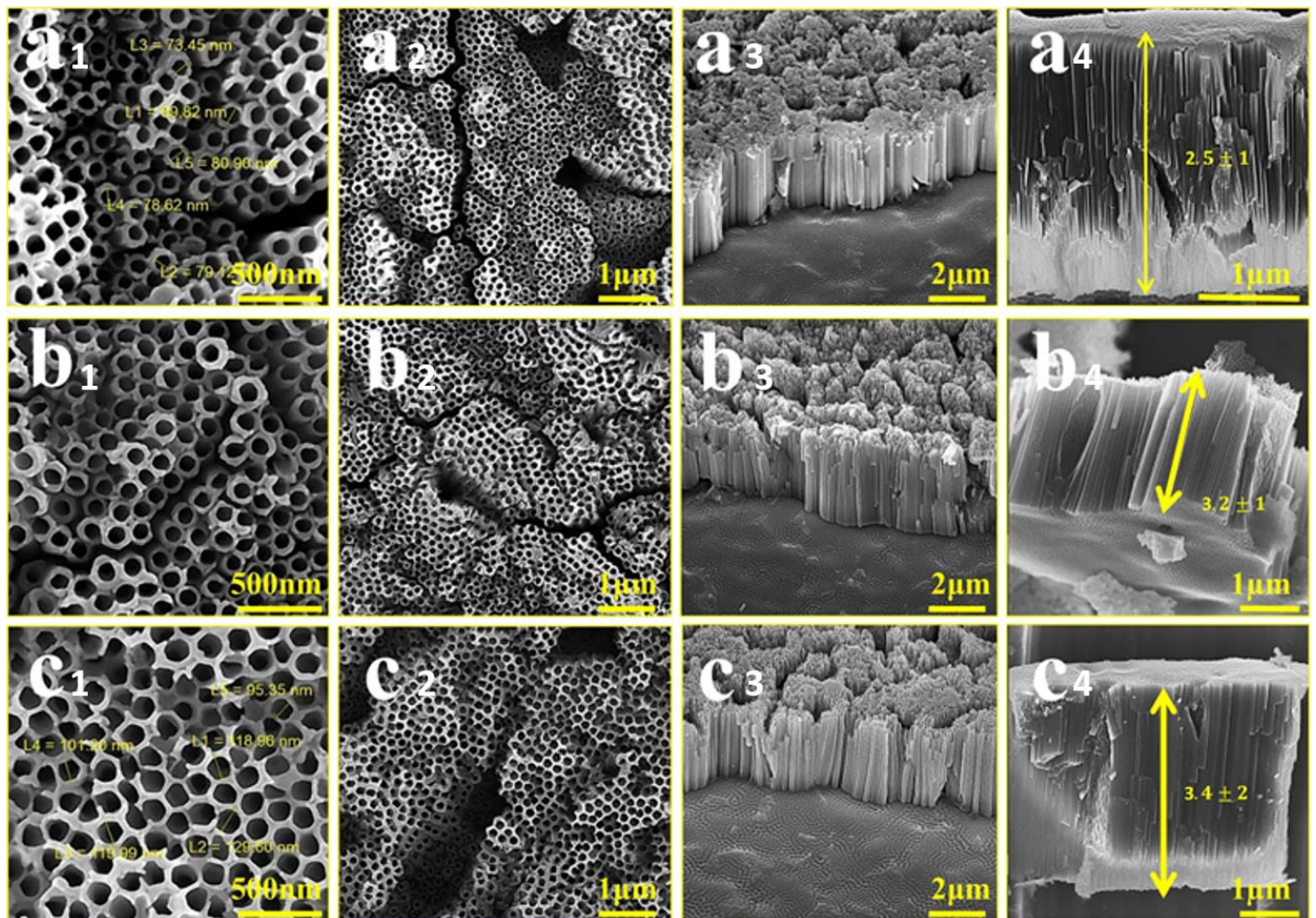


**Figure 1.** Morphology of Ti 6–4 surface after anodizing process under voltage of (a) 50, (b) 60, and (c) 75 V. Reproduced from [25] with permission from Elsevier™.

Here, we present an update on the fabrication of TNTs via the electrochemical anodization technique, focusing on studies that have appeared in approximately the last 15 years. We first discuss the physical and mechanical properties of Ti followed by the effect of alloying addition on the properties of Ti and the synthesized TNTs. The synthesis of TNTs section considers the preparation of TNTs via template-assisted, hydrothermal, and electrochemical anodization methods. Electrochemical anodization is discussed in detail by considering the various factors controlling the dimensions and properties of the synthesized TNTs. Finally, emerging applications of TNT-based materials prepared by electrochemical anodization are highlighted in the applications of TNTs section.

## 2. Fabrication of TiO<sub>2</sub> Nanotubes

Titania nanotubes can be fabricated from different routes, such as the sol–gel process [34,35], vapor–liquid–solid (VLS) growth [36], template-assisted growth [37,38], and hydrothermal [39,40] and electrochemical anodizing methods [41–43]. Each of the processes has its own merits and demerits, but electrochemical anodizing is easy to run and has the liberty to control process parameters to attain a desired set of properties [44–49]. The focus of this review is electrochemical anodizing; hence, anodizing is covered in detail, while an overview of other processes is provided. In



the sol–gel process, a precursor is mixed in a solvent to make a suspended colloidal solution, which form a gel after continuous stirring [50]. Once the desired suspension is achieved, prefabricated templates made from anodized alumina or polymer membranes are immersed in the solution. The suspended particles fill the pores and/or channels of the templates to acquire their shapes. The necessary operations of drying, calcination, and templates/gel removal leave the metal oxide nanowires or nanotubes [34,50]. The particle size and dimensions of the nanostructures depend on the template on which the particle deposited, composition of the colloidal solution, temperature, and time of the deposition. The nanostructures produced from the sol–gel methods are often in a bundled form, which limits the usefulness of the nanostructures [35,51]. The process required to separate the nanostructure from the template material also affects the morphology of the product material [49–52].

In the template-assisted method, nanostructure fabrication can be supported by electrochemical deposition (Figure 2) [53]. The metal oxide or metal is directly deposited to a template and then treated afterwards to produce nanotubes. Both the template and electrolyte affect the oxide structure and morphologies of the produced material [54]. The process has the same drawbacks of non-uniformity and defective morphologies as those of the sol–gel process [34,55,56].

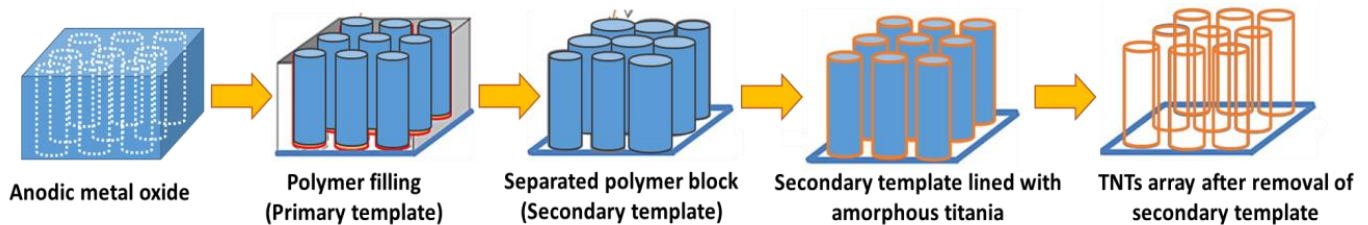


Figure 2. Synthesis of TNTs via template-assisted method.

The VLS is a catalyst-assisted deposition where gaseous reactants dissolve into a liquid metal catalyst (Figure 3) [53]. The liquid metal essentially provides favorable sites for absorption as compared to the slow vapor–solid phase. The nucleation starts within the liquid metal as reactants condense on the liquid metal. Once the nucleation starts within the liquid metal, the growth of a single crystal material proceeds [36]. The VLS is a popular growth method for producing uniform nanowires. In the case of TNT fabrication, the vapor phase is generated by thermal evaporation of Ti metal, which is later allowed to condensate on the liquid gold catalyst. The diameter of the nanotubes is dictated by the size of the catalyst droplet, and their growth is controlled by the temperature and pressure of the system. Although the VLS process is a highly controlled process, it is complex and requires a vacuum environment for fast growth. The temperature is another barrier, as very high temperatures are needed for metal oxides [36,53].

In the hydrothermal process, a nanostructure is grown from aqueous soluble metal salts (Figure 4) [40]. A desired concentration of the metal salt is dissolved in the water and heated from 100 to 300 °C under pressure [39]. The titania powder dissolved in alkaline solution can be used as a precursor material for producing TNTs [57]. The morphology of the titania is controlled by the precursor material, the concentration of the precursor material, temperature, and process time. It is hard to produce nanomaterials with consistent structures and morphologies in the hydrothermal process. The process also requires high temperatures and processing time for nanofabrication [39,40,57,58].

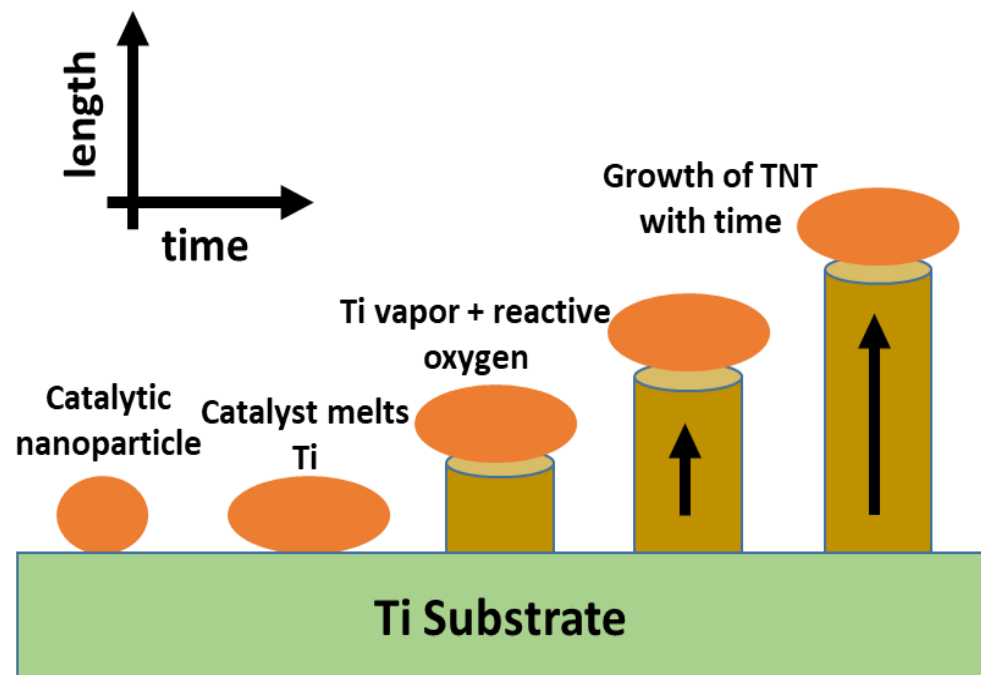


Figure 3. Synthesis of TNTs via catalyst-assisted VLS.

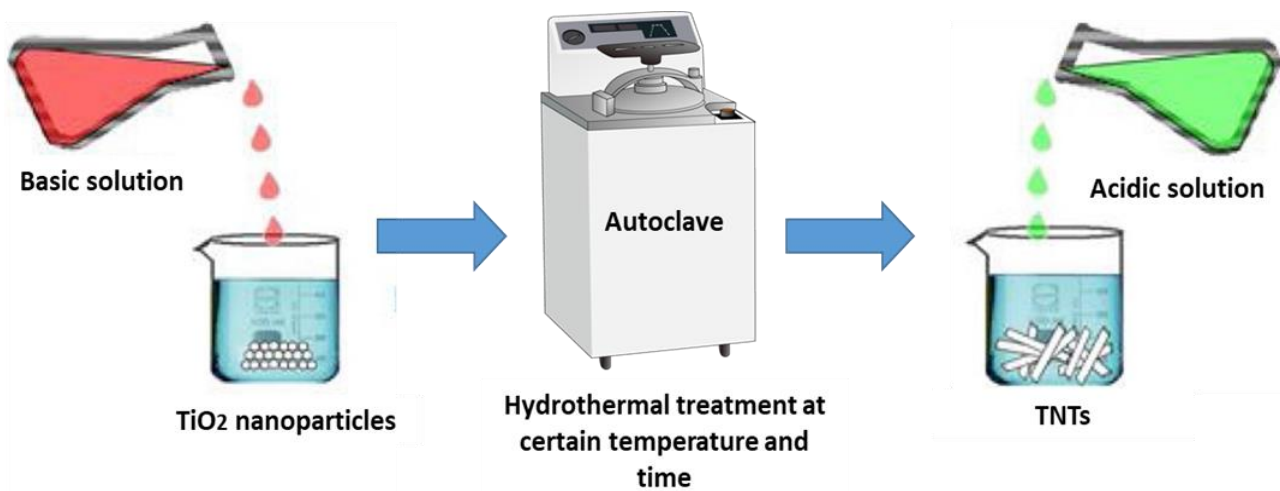
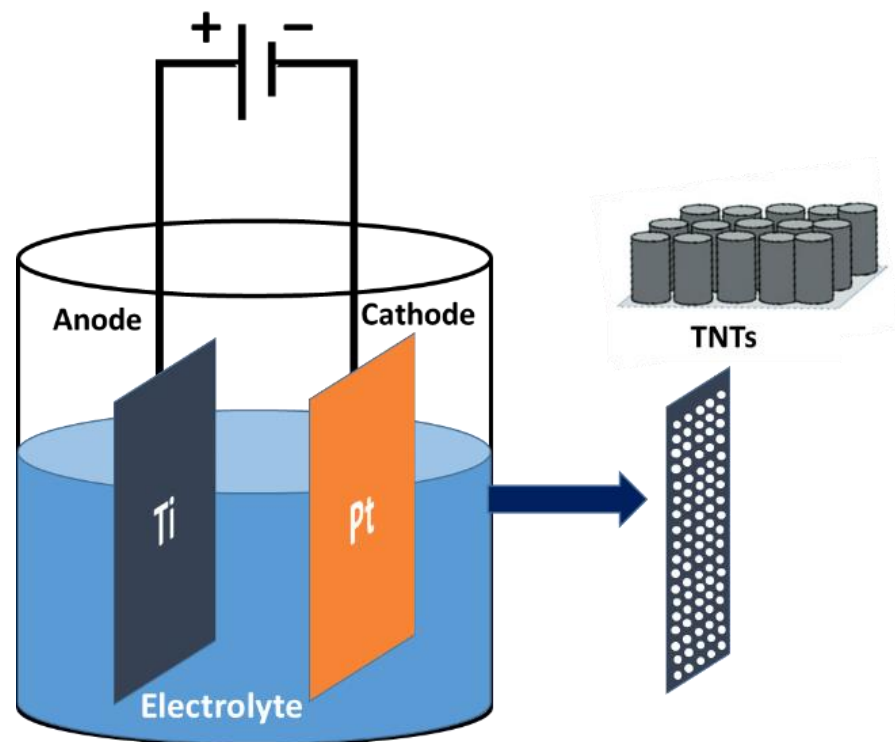


Figure 4. Synthesis of TNTs via hydrothermal treatment.

In electrochemical anodizing, the process involves immersion of the metal in an appropriate electrolyte, which is then anodized at constant voltage for a set duration (Figure 5) [59]. The electrochemical anodizing process provides a high degree of control of the physico-chemical properties of nanotubes by tuning process parameters such as pH, electrolyte chemistry, applied voltage, etc. [44,49,60]. Tuning nanotube properties by adjusting these parameters will be discussed in detail in a later section. The electrochemical anodizing process is easy and inexpensive as compared to other nanotube fabrication processes, where we need vacuum and high processing temperatures. Several research reports have also indicated that the nanotube architecture achieved from electrochemical anodizing possesses unique mechanical, photovoltaic, biomedical, and semi-conducting properties that are not possible to obtain by other methods [44,49,60,61].



**Figure 5.** Synthesis of TNTs via electrochemical anodization.

The electrochemical anodizing setup for titania fabrication consists of two electrodes, an electrolyte, and an external DC source to provide a controlled voltage. The Ti foil or thin Ti sheet where nanotubes grow is connected to the positive terminal, while graphite or platinum is connected to the negative terminal [29,59]. Due to this arrangement, the predominant oxidation of Ti occurs at the anode and hydrogen evolution/oxygen reduction occurs at the Pt electrode. The electrolyte solution consists of variant solvents from deionized water to ethylene glycol or a mixture of both, and the anions include bromide, chloride, fluoride, and sulfates with different molar concentrations of salts [44,45,62]. The process can be carried out at a constant potential (potentiostatic) mode, constant current (galvanostatic) mode, or with a gradual increase in the potential (potentiodynamic) or current (galvanodynamic). As constant potential provides more uniform and self-organized nanotubes, a majority of the anodizing work is reported at a constant potential mode ranging from 6 V to 60 V [55,63–65]. Table 1 summarizes some advantages and disadvantages of the fabrication processes for TNTs mentioned above.

**Table 1.** Comparison of various fabrication processes for TNTs.

Process	Benefits	Drawbacks	Ref.
Sol-gel	<ul style="list-style-type: none"> <li>• Lower synthesis temperature</li> <li>• Highly pure TNTs</li> </ul>	<ul style="list-style-type: none"> <li>• Difficult to scale-up</li> <li>• Time-consuming process</li> <li>• Formation of secondary phases</li> <li>• Uncontrollable aspect ratio of TNTs</li> </ul>	[34,35]
Template-assisted	<ul style="list-style-type: none"> <li>• Broad range of dimensions</li> <li>• Highly uniform, ordered, and vertically aligned TNTs</li> <li>• Compatible with a large number of substrates</li> </ul>	<ul style="list-style-type: none"> <li>• Difficult prefabrication and removal of template</li> <li>• Impurities in TNTs</li> </ul>	[37,38,53]

Table 1. Cont.

Process	Benefits	Drawbacks	Ref.
Hydrothermal	<ul style="list-style-type: none"> <li>• Wide range of temperature for wide range of reactions</li> <li>• Controlled composition of reactants</li> </ul>	<ul style="list-style-type: none"> <li>• Require high pressure</li> <li>• Random distribution of TNTs</li> </ul>	[39,40]
VLS growth	<ul style="list-style-type: none"> <li>• Oriented TNT arrays</li> <li>• Controllable growth direction</li> <li>• Exposed crystal facets</li> </ul>	<ul style="list-style-type: none"> <li>• Require high temperatures</li> <li>• High cost of production</li> <li>• Low through output</li> </ul>	[36]
Electrochemical anodization	<ul style="list-style-type: none"> <li>• Relatively simple and easy to handle</li> <li>• Impurity-free TNTs</li> <li>• Efficient and controlled process</li> <li>• Ordered and vertically aligned TNTs</li> <li>• High aspect ratio of TNTs</li> <li>• Low-cost process</li> </ul>	<ul style="list-style-type: none"> <li>• Incompatible with various substrates including silicon and glass</li> </ul>	[37,41,42,47]

### 2.1. Mechanisms in TNT Formation during Anodizing

The anodizing process takes place in the following steps: (1) oxidation takes place at the metal–oxide interface; (2) hydrogen evolution or oxygen reduction takes place at the cathode; and (3) the voltage drive causes outward migration of metal ions through the oxide–electrolyte interface and inward migration of  $O_2^-$  from electrolyte–oxide interface to the metal–oxide surface [66]. It is largely reported that anodizing takes place due to the initiation of micro/nanopores and their growth related to confined variations of electrochemical environments [29,67,68].

The pore initiation is generally attributed to pitting, which is a localized attack on heterogenous sites. Only few studies provide insight into pore initiation, where they consider the phenomenon occurring at the liquid–solid interface [36,55]. In the case of any liquid–solid interfacial growth, the phase boundary goes under constant microscopic fluctuations. In the case of any electrochemical reaction, these fluctuations can be positive or negative voltage perturbations. A positive perturbation causes bumps, while a negative perturbation causes dents on the interface. The development of these perturbations is attributed either to the composition gradient at the metal–oxide or /and oxide–electrolyte interface or a variation of electrochemical species produced at these interfaces. In the case of anodizing, a dent is produced on the oxide due to negative perturbation to initiate a pore [55].

In the literature, two major hypotheses exist for the growth of nanotubes, namely, fast dissolution inside of the micropore as compared to the edges of the pores and strain energy of compressive forces developed due to electrostatic, electrostriction, and metal-to-oxide volume expansion [43,69,70]. In the fast dissolution theory, the pore-initiating site is very small as compared to the surrounding oxide; hence, the release of cations is very fast inside of the pore, which causes the electrolyte inside the pore to be highly acidified and drops the pH. This causes higher dissolution inside the pore as compared to outside of the pore. The strain energy theory for TNT growth is based on the higher energy zone created due to the excess of positive and negative charges at the interface alongside the volume expansion during the formation of an oxide from metal [69]. This strain energy in return produces highly self-organized nanotubes on the Ti surface [68,70].

## 2.2. Parameters Effecting Properties of Nanotubes

The diameter to length ratio of the nanotubes, horizontal and vertical ordering of the nanotubes, and the wall thickness of the nanotubes contribute to the morphology and structural properties. It is of significant interest to acquire a set of properties of TNTs by altering anodizing process parameters [44,46,48]. The major parameters that control the properties in the anodizing process include the voltage drive between the anode and cathode, the electrolyte used during the process, the temperature of the electrolyte bath, and time given for the anodizing [45,48,63,65]. The surface preparation of the substrate, composition at the surface, and supporting salts in the electrolyte also contribute towards controlling properties of the nanotubes [45,58,62,67].

The applied voltage in anodizing, generally called the potential window, is one of the key factors in controlling the diameters of the nanotubes [71]. At low voltage, the oxide dissolution is low; hence, nanotubes grown at very low voltages have small diameters. Although the reported work suggests that the voltage, electrolyte, and temperature contribute to determining the diameter and thickness of the nanotubes, some of the research reported a linear relationship between the diameter and thickness of the TNTs and the potential windows [48,65,72]. The potential windows are reported to be 10–25 V in the literature for aqua-base electrolytes, while in organic electrolytes, the window can be extended to several hundred volts. However, most of the researchers used a potential window of 20–70 V. To tune the diameter, wall thickness, and variation in the diameter of nanotubes from the bottom to the top, researchers carried out anodizing in the potentiostatic, potentiostatic with negative voltage pulse, and potentiodynamic modes. Relatively consistent diameters of nanotubes were reported in the potentiostatic mode, and the thickness control of the double-walled nanotubes with negative voltage pulse yielded better photovoltaic properties, while a gradual increase in the voltage (potentiodynamic) yielded a gradual rise in the nanotubes' diameter from the bottom to the top of the nanotubes [73]. The TNT growth at lower field strength (V/cm) is controlled by ohmic processes, while at high voltage, strength is driven by the migration processes taking place in anodizing [65,71].

Time for anodizing is another important parameter to control the thickness of TNTs [74]. The reported experimental time for anodizing is from a few minutes to several hours. A short anodizing time produces a spongy structure with no clear identification of nanotubes, while greater time produces a more defined, thicker nanotube structure. The growth rate is fast at the start and slows down with time. A study reported that nanotube growth in a fluoride-containing electrolyte at 40 V was 1  $\mu\text{m}$  after 30 min and increased by 3  $\mu\text{m}$  after 15 h of anodizing [45,74]. The fast growth at the start is attributed to dissolution due to an excess of anions and migration of cations from inside of the nanotubes. Once a steady state is achieved between dissolution and oxidation, the growth of nanotubes slows down. The metal to oxide layer, which is also called the compact layer, is largely dependent on the voltage drive, while the growth at oxide–electrolyte increases with time. The longer the time of anodizing, the greater the thickness of the nanotubes [45,74,75]. It is also worth mentioning here that more organized nanotubes can be achieved if sonication is carried out of the compact layer or if initial porous or disoriented nanotubes are removed by adhesive tape.

The tuning of electrolytes used in the anodizing process greatly contributes to engineering the structure and properties of nanotubes [75,76]. Within the electrolyte bath, the type of electrolyte, its pH, constituents of the electrolyte, the viscosity of electrolyte, and dissolved oxygen all affect the architecture of the nanotubes. There are four distinct generations that exist for nanotube formation in hydrofluoric acid (HF)-based aqueous solution, buffered electrolytes, organic electrolytes, and fluoride-free electrolytes [76]. The HF-based aqueous solution is highly acidic, where the pH of the solution is very low; this results in chemical dissolution of titania by fluoride ions as an anodizing rate-controlling step. The oxide dissolution by fluoride ions achieves dynamic equilibrium very fast. Although the nanotubes formed in HF-based electrolytes were organized,



their length was restricted to less than 1  $\mu\text{m}$  thickness. In buffered electrolytes, a weak acid such as KF or NaF can be added to the electrolyte to decrease the acidity of the electrolyte. By adjusting the pH to around 4.5, a thickness of around 4.4  $\mu\text{m}$  can be achieved for the nanotubes. The addition of a weak acid slow down the oxide dissolution; hence, it takes a longer time to achieve dynamic equilibrium. Further increases in the pH to the neutral level increase the nanotube length but incorporate unwanted complexes entangled within the nanotube structures. The dissolution of titania can also be slowed down by using a more viscous electrolyte such as glycerol, ethylene glycol, diethylene glycol, etc. [40,76]. A more efficient dissolution control of the titania allows the formation of more organized, longer nanotubes. Nanotubes of a length of 134  $\mu\text{m}$  were reported in ethylene glycol electrolyte containing 0.25%  $\text{NH}_4\text{F}$  at 60 V for a period of 17 h. The growth can be enhanced by adding a small amount of water (5% by volume). A length of 250  $\mu\text{m}$  was achieved by adding 0.18 wt.% water, while much longer nanotubes of 1000  $\mu\text{m}$  were achieved in ethylene glycol containing 0.6%  $\text{NH}_4\text{F}$  and 3.5% water at 60 V after 216 h. The high viscosity and strong oxygen bond in organic electrolytes slow down the dissolution and formation of TNTs. A small amount of water assists both processes and helps in producing longer nanotubes. Non-fluoride electrolytes such as hydrochloric acid, phosphoric acid, etc. are also used to achieve self-organized nanotubes at much lower voltages as compared to those used in fluoride environments [59,70,77,78].

The above-mentioned electrolyte systems produce anodized nanotubes of a short compact layer and a relatively thicker outer layer. The nanotube structures produced in deionized water and sulfide-containing electrolytes are more compact [76]. The structures grown at low voltages in water are not reported to be nanotubular but rather nanorods or nanofibers. At higher voltages, a porous nanostructure appears with ridges and serrations on the nanotube edges. The nanotubes grown in sulfuric acid and sodium sulfide are reported to be more compact with a disoriented structure [75].

The temperature of the bath is another factor for controlling the properties of nanotubes [61]. The reaction rate generally increases with increased temperature; hence, the wall thickness of the nanotubes and their length increase with temperature. The temperature of the electrolyte in both aqueous and organic electrolytes contributes due to the increase in oxidation and decrease in viscosity [58]. The reported work suggests that in aqueous solutions, there is an inward thickness increase in the case of an aqueous electrolyte system due to higher oxidation at higher temperatures. An outward thickness increase of the nanotubes is reported in non-aqueous fluoride-containing electrolytes, probably due to decreases in the viscosity, which increase the mobility of fluoride ions. More organized layers are reported at 5  $^\circ\text{C}$  for aqueous solutions, and more organized and longer nanotubes are reported for non-aqueous solutions around 505  $^\circ\text{C}$  [58,61].

### 2.3. Properties Modification of Nanotubes

The TNT structure produced after the anodizing process is amorphous, which is not a very desirable structure for photovoltaic and electrical applications [79]. The amorphous structure can be easily tailored to the crystalline structure by annealing within a temperature range of 250–300  $^\circ\text{C}$ . The annealing process further allows the control of nanotubes' dimensions by providing a surrounding gaseous environment [63,80]. Anodizing takes place in an aqueous solution, which causes the interior of the nanotubes to be rich in hydroxide as compared to the exterior of the nanotubes, and this defect can also be eliminated by the annealing process. The crystallization of TNTs depends on the annealing temperature; above 300  $^\circ\text{C}$ , the anatase–rutile structure is formed, and further increases in the temperature cause the complete transition to anatase [81]. If the temperature is raised beyond 500  $^\circ\text{C}$ , the anatase structure starts converting to the rutile phase. The nanotube structure obtained at 350  $^\circ\text{C}$  is the highest-conducting structure in annealing and is preferred for photovoltaic properties. It has been further reported that annealing to 650  $^\circ\text{C}$  in argon gas transfers the bottoms of the nanotubes to rutile while keeping the top-end of the nanotubes

at the anatase phase, which enhances the photovoltaic property even more as compared to that achieved at 350 °C [58,61]. The high photovoltaic property in the mix phase is attributed to the lower band gap of the rutile phase (3.0 eV) as compared to the anatase phase (3.2 eV), which allows the absorption of a wider range of wavelength, i.e., <378 nm to <413 nm. The transformation of an amorphous anodized nanotube structure to anatase and rutile as a function of temperature was also studied in situ by Zeng et al. [75]. They confirmed the initial transformation of anatase from 350–400 °C and further conversion to the rutile phase at 650 °C. They also reported the elimination of structural defects after anodizing by annealing. The reducing environment of ammonia and hydrogen gas has also been studied by researchers to tune the wall thickness of TNTs, modifying the properties of the double-walled nanotubes [61,79,80].

It can be summarized from above that anodizing is a simple and versatile process for the fabrication of TNTs; alteration of process parameters allows the fabrication of specific structures and morphologies. The physico-chemical properties of a nanostructure are directly related to its structure and morphologies; hence, this can be controlled by adjusting process parameters.

### 3. TNT Application in Solar Cells

TNTs have been widely investigated over the last several decades for their possible applicability in solar cells, as they can be used in conjunction with other technologies that are now in use [82–84]. Continual progress has been made in the fabrication and modification of the TiO<sub>2</sub> structure, resulting in the development of novel properties and applications in the photovoltaic area, particularly in the field of solar energy conversion. Although newly created devices based on this novel idea have substantially expanded the variety of applications of TiO<sub>2</sub>, this expansion has also resulted in new demands being placed on the physical qualities of the material. The application of TNTs to photovoltaics has made significant strides in recent years, with dye-sensitized solar cells [85–87], polymer-inorganic hybrid solar cells [88–90], and perovskites [91–93] among the most notable.

TiO<sub>2</sub> nanomaterials are suitable materials for solar cell applications owing to their high optical and chemical stability, non-toxicity, corrosion resistance, and low cost [83,94]. TiO<sub>2</sub> naturally exists in four commonly known polymorphs, i.e., rutile (tetragonal), anatase (tetragonal), brookite (orthorhombic), and TiO<sub>2</sub> (B) monoclinic [95–97]. When it comes to solar cell applications, it is recommended to use the anatase structure over other polymorphs because it has the potential to have a higher conduction band edge energy and a lower recombination rate of electron–hole pairs than other polymorphs [98]. Although TiO<sub>2</sub> nanocrystals have an intrinsic electronic structure, their physical and chemical properties are influenced by their size, shape, structure, and surface characteristics. Recent advances in nanostructured TiO<sub>2</sub> materials, such as nanorods, nanotubes, nanosheets, nanofibers, and linked structures, have piqued the interest of researchers, who have developed and implemented a variety of nanostructured TiO<sub>2</sub> materials in photovoltaic systems [99–104].

The most common application of nanostructured titania has been in dye-sensitized solar cells (DSSCs), which are considered to be among the most promising of the various third-generation photovoltaic technologies now under development [105]. When compared to conventional silicon-based solar cells, DSSCs have a higher solar energy conversion efficiency (>10 percent) because they have a simpler structure, a more scalable production technology, and lower manufacturing costs [106,107]. DSSCs generally consist of an n-type semiconductor with a large band gap that works as an electron conductor coated with dye, a liquid electrolyte for hole conduction, and at least two transparent conducting electrodes, such as conductive fluorine tin oxide-coated glass, to form a closed circuit as shown in Figure 6. In DSSCs, the photovoltaic process starts at the semiconductor/dye interface. The light excites the electrons in the dye, which are quickly transported to the semiconductor's conduction band. Because of its superb physical and chemical properties, titanium dioxide (TiO<sub>2</sub>) is by far the most extensively used semiconductor. The electrons flow through the external load and return to the counter electrode, which is in direct contact with the liquid

electrolyte, where they are absorbed. The ionic transport of a redox pair in the electrolyte is responsible for the regeneration of the dye.

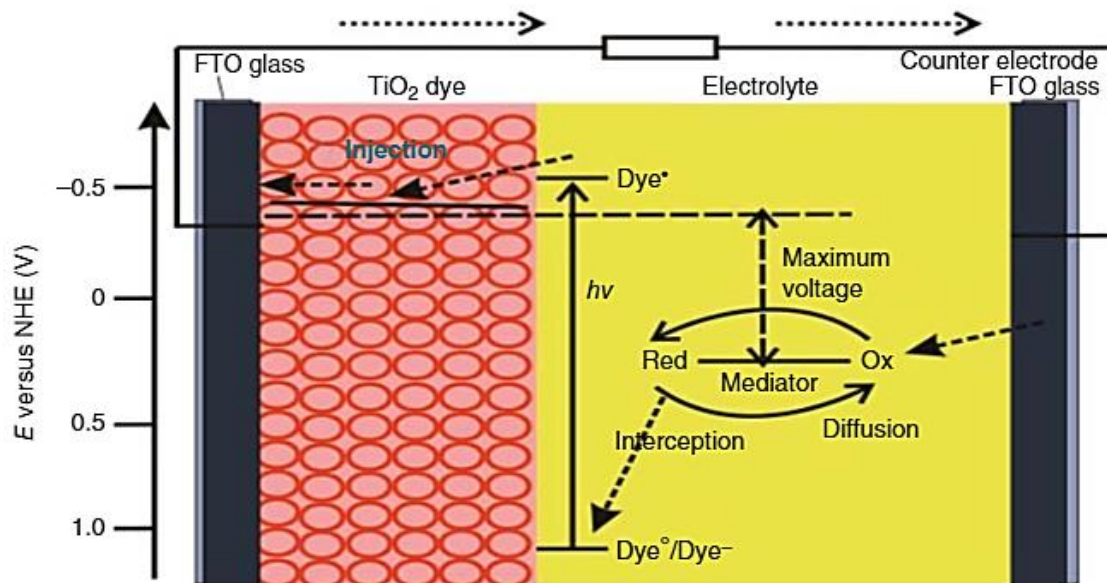


**Figure 6.** Schematic diagram of the working principle of DSSCs. Reproduced from [108].

The nanocrystalline structure of  $\text{TiO}_2$  is critical for the efficient operation of DSSCs [109]. Because ordered one-dimensional nanostructures such as nanotubes, nanorods, and nanowires are expected to provide direct charge transport routes and thus the boost charge-collecting efficiency of DSSCs, much research has focused on photoanodes made of these nanostructures [83]. TNTs are thought to perform better compared to other one-dimensional nanostructures (i.e., nanowires and nanorods) due to their larger surface area provided by their hollow structure. The one-dimensional structure of TNTs enables efficient electron conduction without intergranular scattering, which is common in other nanostructured materials [110,111]. The charge-collection efficiency has also increased because of the faster recombination time offered by TNTs. The use of TNTs also allows efficient light trapping and deeper light penetration due to their long electron diffusion length and hollow shape.

Recent research has focused on polymer–inorganic hybrid solar cells, which have the potential to become another low-cost and significant source of solar energy conversion [89,90,112]. They combine the best semiconductor features, such as high electron mobility and stability, with the operational flexibility given by polymers. Light is absorbed by the polymer in these devices, resulting in the formation of excitons. Upon reaching the hybrid interface, excitons break and split into independent charges, which introduce electrons and free holes into the inorganic semiconductor and the polymers, respectively. The use of TNTs as a semiconductor material in these solar cells can improve performance and reduce costs [113,114]. The polymers occupy the empty space between arranged TNTs and form hybrid active layers. TNTs have an organized nanostructure, which allows the creation of direct charge transport pathways in these devices. Mor et al. [115] showed a hybrid device made of TNT arrays sensitized with SQ-1 and uniformly infiltrated with p-type 3-hexylthiophene-2,5-diyl (P3HT) as shown in Figure 7. The vertical TNT arrays with 20–35 nm pore sizes allow for efficient charge production and P3HT infiltration within the tubes. In this arrangement, SQ-1 dye absorbs red and near-IR photons, while P3HT harvests higher energy photons. The comparable absorption bands of these two materials make them suitable candidates for a wide-spectrum solar cell. As a result, the efficiency of the device increased to 3.8% in AM 1.5 full sunshine.

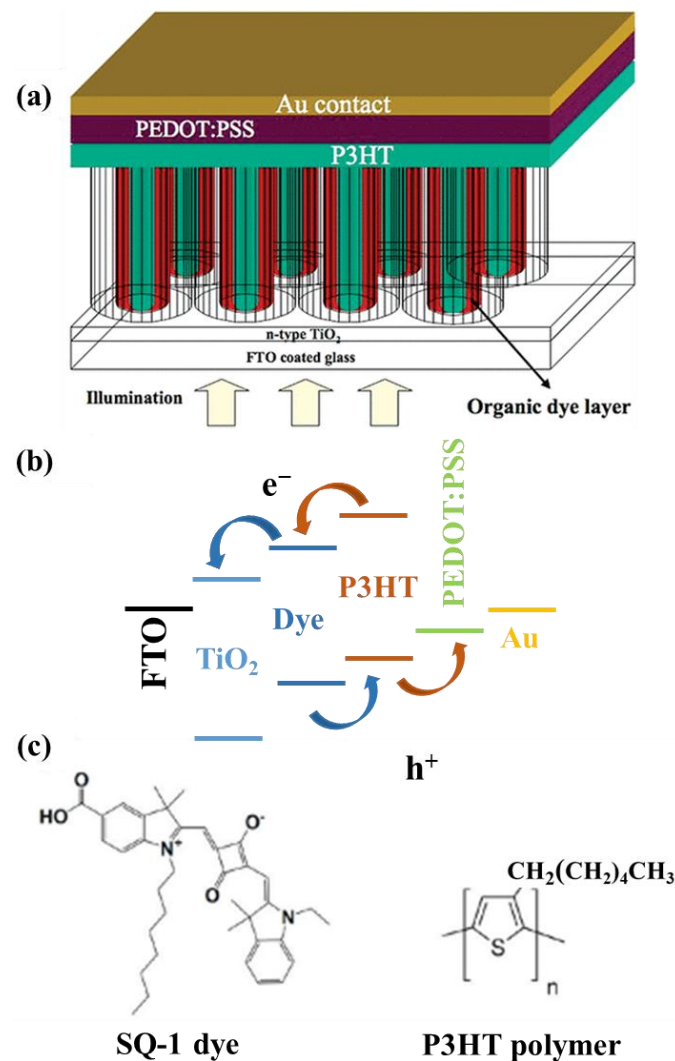


**Figure 7.** (a) Depiction of hybrid solid-state solar cell, (b) Energy level positions and charge transfer processes of the constituent layers of the described hybrid solar cell, (c) Molecular structure of SQ-1 dye and P3HT polymer. Adapted from [115] with permission from American Chemical Society™.

Perovskite is a new class of light harvesters for mesoscopic solar cells that has recently drawn a lot of interest [92,93]. It only took a few years for this newly constructed solar cell to acquire a power conversion efficiency (PCE) of 15.4%. Javed et al. [91] recently revealed that encapsulating TNTs with Cs nanoparticles improves the performance of PSC by increasing the electron injection rate and thermal stability of the device. A simple electrochemical anodization method was employed to synthesize TNTs and Cs-TNTs in their study. The Cs-TNTs displayed significant absorption when compared to the pure TNT sample, with the doped sample exhibiting a red shift in the spectrum. When compared to a pure TNT-based electron transport layer in perovskite solar cells, the Cs-TNT-based perovskite device performed better, resulting in an 18.67% and a 22.28% increase in JSC and PCE values, respectively. Increased extraction of photo-generated charge carriers in the device could be a reason for the reported improvement in photovoltaic characteristics.

As a result of these consistent advancements, it has become clear that TNTs are one of the vital nanostructured materials in the hunt for efficient and low-cost solar energy conversion solutions. It is envisaged that future research efforts on novel materials and critical interfaces will lead to the creation of TNT-based solar cells.



#### 4. TNTs for Biomedical Applications

Among many other disciplines, TNTs have had appeal in the biomedical field. As titania is non-toxic in the human body and possesses better corrosion resistance and high specific strength, it has become one of the most widely used biomaterials for orthopedics, dental implants, bone regeneration, and smart drug delivery systems [47,116]. Titania is either being utilized in the form of a coating on an implant material through various deposition techniques or by growing self-ordered arrays of TNTs on a Ti substrate via the electrochemical anodization process [16,23].

Targeted drug delivery is a promising approach for sustained and efficacious release of antibiotics and other drugs, applicable in both oral drug administration and implanted devices. One such example is the study conducted by Mansoorianfar and coworkers [25]. Electrochemically anodized TNTs were filled with the antibacterial drug vancomycin on the implant surface, first by immersion and then by the electrophoresis method. The vancomycin particles released from TNTs and attached to bacteria, hindering bacteria from forming an infectious biofilm on the implant surface.

Figure 8 illustrates the antibacterial mechanism of TNTs via different modes described by Li et al. [117]. The bacterial inhibition modes can include: charge repulsion antibacterial property (A), stretching force antibacterial property (B), hydrophilicity prohibiting bacterial adhesion (C), controlling drug release and loading quantity via regulation of the dimensions (D), controlling drug release via the application of coatings (E), controlling drug release and loading quantity via the use of drug-mixing coatings (F), distribution of NP and ion release ability of a TNT modified by polydopamine-assisted reduction (G), distribution of NP and ion release ability of a TNT modified by magnetron sputtering (H), distribution of NP and ion release ability of a TNT modified by ion implantation (I), the pH-triggered self-response system (J), the temperature-triggered self-response system (K), and the enzyme-triggered self-response system (L).

There are certain features required of a biomaterial to contemplate its use in orthopedic practices and dentistry. Just like any other implant or organ replacement in the body, dental implants too significantly depend on their safe, stable, and long-term bonding with the jaw bone. The dental implant should be able to positively interact with fibrous connective tissue to set off as biofunctional.

A biocompatible material harboring attractive mechanical characteristics specific to the site of application is a fundamental requirement. Along with that, resistance to corrosion and wear in the human physiological environment and good osseointegration are the prerequisites for a suitable orthopedic and dental implant [118,119]. Ti and its alloys have been identified as suitable choices for this purpose [25,120]. To enhance the interaction of Ti-based implants with the bone, various surface treatment techniques have evolved over time, including grit blasting, acid etching, incorporation of metallic ions in TNTs, and electrochemical treatment [121,122]. It is an established fact that osteoblast proliferation is critical for bone regeneration and that TNTs can promote it. Chernozem et al. and coworkers fabricated TNTs on a Ti–Nb substrate at two different anodization voltages with varying Nb content, as Nb is inert and biocompatible. Better results for mesenchymal stem cell (MSC) adhesion and cell proliferation were obtained at a lower voltage, irrespective of the Nb content [21]. A major portion of the human bone is made up of hydroxyapatite (HA), a natural mineral of Ca, P, and O. For an implant to bond with bone tissues, HA promotes the necessary interaction [123]. Many investigations are considered successful on the ability of a material to produce HA. An *in vitro* study in SBF was conducted to analyze the bioactivity of MnO–NPs decorated in anodized TNTs [124]. A higher amount of HA was formed in TNTs decorated with a higher concentration of MnO–NPs.

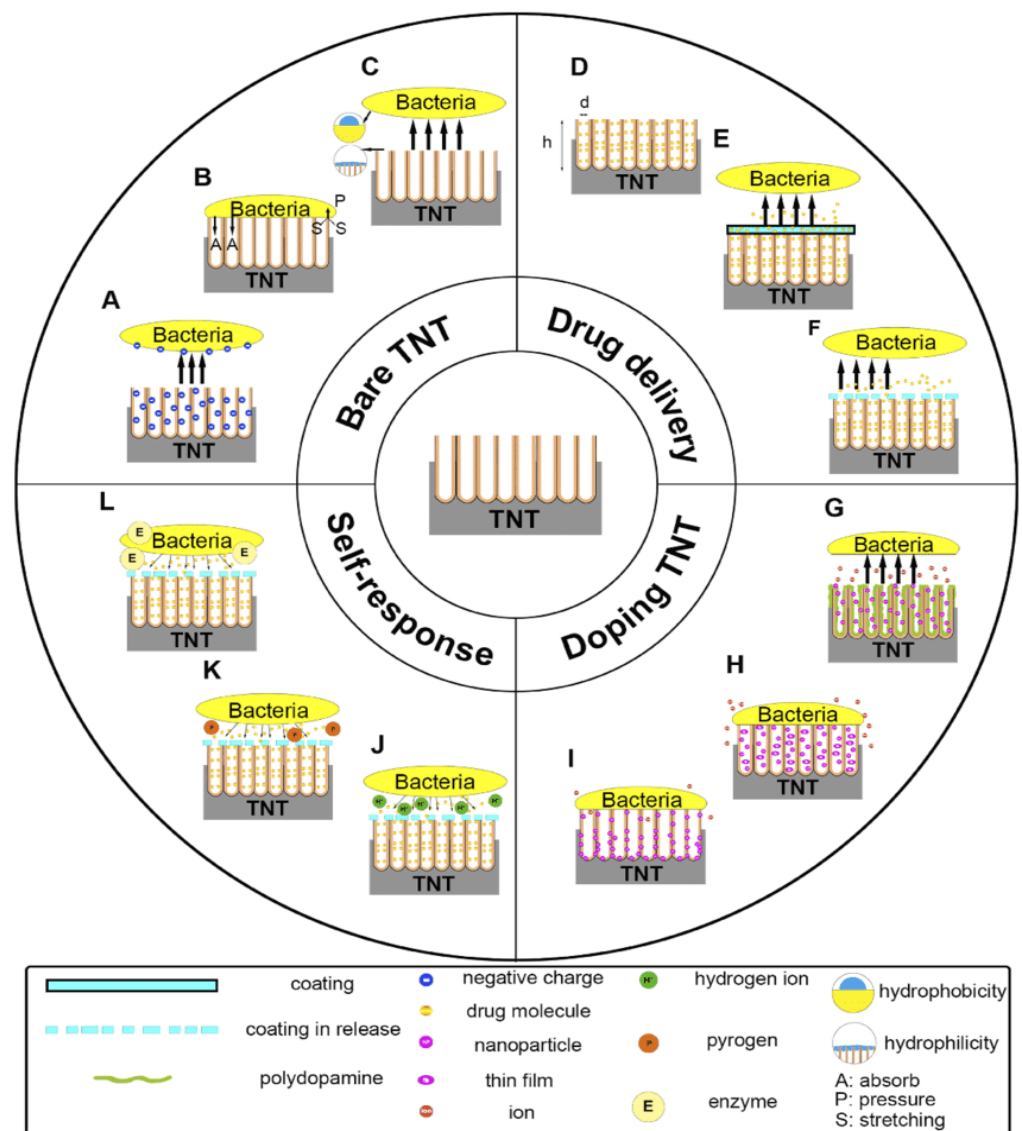


**Figure 8.** Mechanisms of antibacterial application of TNTs in orthopedic implants. Reproduced from [117].

Targeted drug delivery and control over drug releasing capability are the key features to augment the therapeutic effect in clinical trials, and TNTs are potential candidates for the occasion [125]. Owing to the tubular structure formation and high surface area, there is ample space for various drug loadings in TNTs. Such a system for the antibiotic gentamicin, loaded in electrochemically synthesized TNTs on Ti–24Zr–10Nb–2Sn was explored by Lopez and his group [126]. The study aimed at the bactericidal effect of the antibiotic and its sustained release in the phosphate buffer solution. The results showed an effective release of the drug from TNTs in an antibiogram test, which remarkably inhibited the growth of bacteria staphylococcus aureus in the culture medium.

The beneficial drug-carrying capacity of TNTs has played a significant role in the advancement of chemotherapy without damaging healthy cells. The localized release of the anti-cancerous drug cisplatin loaded in chitosan-coated TNTs were probed by Wan and his colleagues [127]. A prolonged release of the drug was reported, challenging the traditional chemotherapeutic treatment for cancer. Other than potential drug carriers, TNTs have found application in cancer treatment through photodynamic therapy (PDT). PDT is an efficient and non-invasive alternate method for treating tumor cells instead of conventional therapies [128]. The mechanism involves the irradiation of a photosensitizer biomaterial

with the help of light, distributed at the site of unhealthy cells as shown in Figure 9 [129]. The photosensitizer absorbs photons of a certain wavelength and enters an excited energy state, leading to the production of reactive oxygen species (ROS), which helps destroy cancer cells. Jimenez et al. [130] synthesized novel folic acid (FA)-conjugated TNTs and alumina NTs to use them as biocompatible photosensitizers in PDT. FA-conjugated TNTs generated a sufficient amount of ROS targeting the HeLa cells, proving their potential future application in PDT. However, intensive research is needed to modify and shift the photodynamic response of TNTs towards the spectrum of visible light.

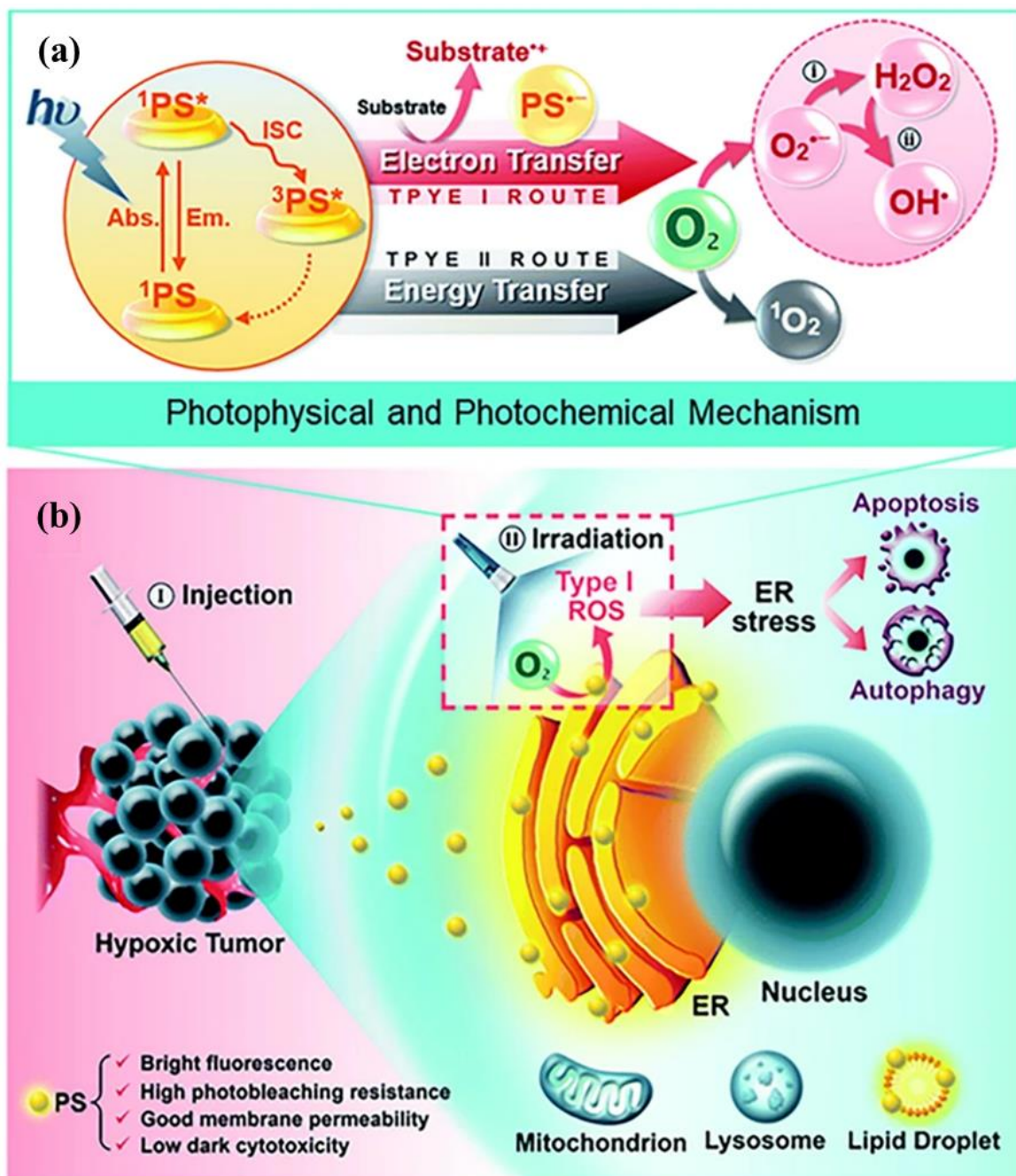


Figure 9. (a) Schematic diagram of the photophysical and photochemical mechanisms, \* represents the excited energy state of PS, (b) The cytological process of PDT therapy. Reproduced from [129].

TNTs have exhibited numerous utilities in the biomedical field mainly due to their astounding biocompatibility and ease to control their physical and chemical properties through various processing techniques. Biomedical applications in the case of TNTs can be categorized as drug delivery systems, antibacterial surfaces, and osseointegration in implanted devices. Decades of research prove that TNTs have established their worth as an efficient, non-toxic, and cost-effective biomaterial. Table 2 comprising a few recent studies in the field of dentistry and orthopedic implants is given below for further reading.

**Table 2.** TNTs application in dentistry and orthopedic implants.

Application	System	Major Findings	Ref.
Dental Implants	<ul style="list-style-type: none"> <li>• Electrochemically anodized TNTs</li> <li>• 3D-printed Ti–6Al–4V substrate with controlled microstructure using selective laser melting</li> <li>• Bioactive coating of HA by immersion method</li> </ul>	<ul style="list-style-type: none"> <li>• Successful synthesis of Ti alloy strips</li> <li>• Improved osseointegration, protein adsorption, and cell adherence and growth</li> </ul>	[131]
	<ul style="list-style-type: none"> <li>• Electrochemically anodized TNTs</li> <li>• Natural resinous compound propolis loaded in TNTs</li> </ul>	<ul style="list-style-type: none"> <li>• Enhanced cell proliferation and differentiation</li> <li>• Propolis was effective as antibacterial and anti-inflammatory drug</li> <li>• Increase in bone mineral density</li> </ul>	[132]
	<ul style="list-style-type: none"> <li>• Anodized TNTs</li> <li>• Loaded with Ag and Zn NPs by DC magnetron sputtering</li> </ul>	<ul style="list-style-type: none"> <li>• Achieved augmented microbial elimination in vitro against <i>S. mutans</i>, <i>Candida albicans</i>, and <i>Candida parapsilosis</i></li> </ul>	[133]
	<ul style="list-style-type: none"> <li>• Modified TNTs using thermal hydrogenation technique, i.e., H<sub>2</sub>–TNTs</li> </ul>	<ul style="list-style-type: none"> <li>• Super-hydrophilic surface was produced over TNTs</li> <li>• Improved bioactivity of HGFs</li> <li>• Improved regeneration of soft connective tissues</li> <li>• Accelerated wound healing capacity of H<sub>2</sub>–TNTs was observed</li> </ul>	[134]
Orthopedic Implants	<ul style="list-style-type: none"> <li>• Electrochemically anodized TNTs</li> <li>• Decorated with Au–NPs by repeated immersion and irradiation process</li> <li>• Layered deposition of Au–NPs</li> </ul>	<ul style="list-style-type: none"> <li>• Successful synthesis of visible light triggered surface</li> <li>• Photocatalytic behavior attained</li> <li>• Good antimicrobial and anti-inflammatory response</li> </ul>	[135]
	<ul style="list-style-type: none"> <li>• Electrically polarized TNTs</li> <li>• CP Ti substrate</li> </ul>	<ul style="list-style-type: none"> <li>• Accelerated bone healing achieved</li> </ul>	[136]
	<ul style="list-style-type: none"> <li>• Electrochemically anodized TNTs</li> <li>• Ag–NPs loading via immersion</li> </ul>	<ul style="list-style-type: none"> <li>• Burst drug release achieved at pH of 5.5, related to infectious site</li> <li>• Increased antibacterial properties shown by Ag–NPs</li> <li>• Novel design did not inhibit osteo-induction</li> </ul>	[137]



Table 2. Cont.

Application	System	Major Findings	Ref.
	<ul style="list-style-type: none"> <li>Electrochemically anodized TNTs</li> <li>Duplex coating of HA–chitosan–casein co-doped with La and Tb via electro-deposition method</li> </ul>	<ul style="list-style-type: none"> <li>Homogeneous novel composite coatings were achieved</li> <li>Apatite formation was favorable in attaining bioactivity and antibacterial response</li> <li>Appreciable protection against corrosion in Ringer’s solution</li> <li>Potentially good choice for orthopedic implants</li> </ul>	[138]
	<ul style="list-style-type: none"> <li>Electrochemically anodized TNTs</li> <li>Antibacterial poly-hexamethylene guanidine (PG) loaded in TNTs via overnight immersion</li> </ul>	<ul style="list-style-type: none"> <li>Superior antibacterial behavior</li> <li>Elimination of <i>E-coli</i> and <i>S. aureus</i> in a 5 min slot only</li> <li>Effective against infection in rat infection model</li> <li>Enhanced osteo-induction</li> </ul>	[139]
	<ul style="list-style-type: none"> <li>HA–TNT–CNT nanocomposites</li> <li>HA–TNT composites (from respective powders) produced via hydrothermal process</li> <li>Incorporation of CNTs in HA–TNT composite by hydrothermal mixing</li> </ul>	<ul style="list-style-type: none"> <li>Improved surface hardness, wear resistance, and Young’s modulus</li> <li>Enhanced adhesion and proliferation of cells</li> <li>No cytotoxicity was exhibited on HA–TNT–CNT surface</li> </ul>	[140]

## 5. TNTs for Water Purification

Another field of applications for TNTs is water purification for producing potable water. The TNTs can either be used for photocatalysis of organic pollutants or as biocidal materials to induce antifouling properties. The nanotubular structure of titania is considered superior over a spherical and cubical shape for both applications due to a higher surface to volume ratio [141]. However, water contamination due to any leaching and the resultant cytotoxicity and genotoxicity should also be considered carefully to ensure biocompatibility.

Photocatalysis essentially utilizes the photon energy from ultraviolet or visible light to degrade organic pollutants through a photo-assisted oxidation reaction. Often, the process of photocatalysis is augmented with the electrochemical oxidation of the organic matter, termed photoelectrocatalysis. These methods of decontaminating water are preferred over traditional biological or other chemical processes due to their lower cost and simplicity. To elaborate further, no chemicals, i.e., simply the electrons, act as the reagents to carry out the desired oxidation reaction.

Titania has proved to be an efficient catalyst for non-selective oxidation of organic impurities in water. A film of TNTs has displayed higher photocatalytic efficiency for oxidation of organic pollutants compared to that of TNPs. Furthermore, it has also been established that the individual TNTs have higher mass and charge transfer capacities than the interconnected TNTs and thus have an improved rate of photo-assisted oxidation of the organic matter. Chemical doping as well as microstructural adjustments has also been considered to improve the performance of TNTs as photocatalysts. However, chemical doping has resulted in a decreased oxidation rate due to decelerated electron transfer and accelerated recombination of electron–hole pairs. Another approach to improve the photocatalytic activity of TNTs for oxidation reaction is to add hydrogen peroxide (H<sub>2</sub>O<sub>2</sub>) in the aqueous media [142].

TNTs have also been utilized to electrochemically reduce chromium hexavalent ions (Cr(VI)) from industrial wastewater into less toxic trivalent ions (Cr(III)). This process was also improved by the use of alkaline urea as an anolyte additive as a result of the release of additional electrons at the anode. Moreover, it was also noticed that the lower concentrations of urea could help with the Cr(VI) reduction to Cr(III), as higher concentrations would lead to polarization losses. Finally, a comparison was made between bare Ti and TNTs used as cathodes, and higher Cr(VI) reduction to Cr(III) was observed [143] as shown in Figure 10.

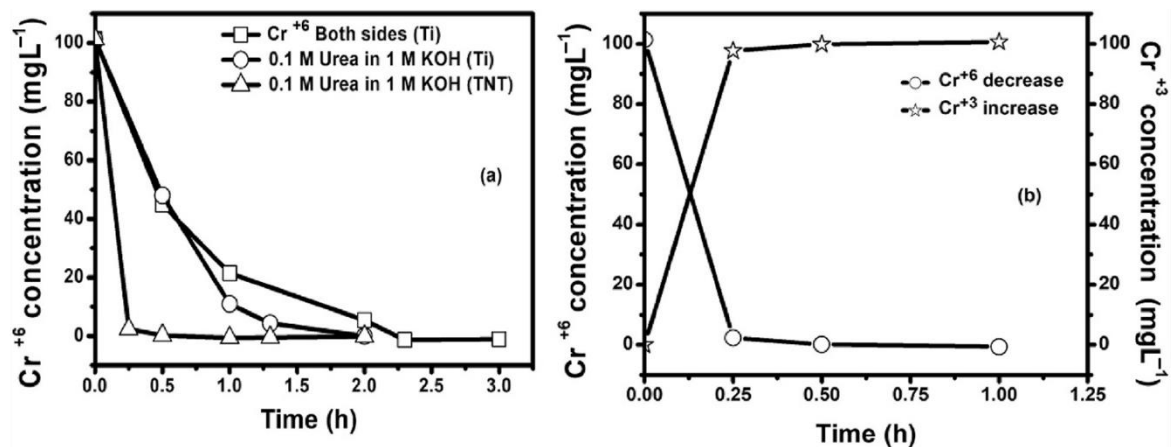


**Figure 10.** (a) Electrolytic reduction of 100 mgL<sup>-1</sup> Cr (VI) at 5 V with (□) Ti cathode with 100 mgL<sup>-1</sup> Cr on both sides, (○) addition of 0.1M urea into 1M KOH at anode and with Ti cathode, (Δ) addition of 0.1 M urea into 1 M KOH at anode and with TNT cathode, (b) Cr (VI) reduction into Cr (III) on TNT with urea as anolyte additive (reproduced from [143] with permission from Elsevier™).

Finally, TNTs also have shown potential against biological microorganisms (i.e., algae and bacteria). For example, Wang et al. [144] studied the toxicity of TNPs, TNTs, and a binary mixture of TNPs and TNTs for two freshwater algae, namely, *Scenedesmus obliquus* and *Chlorella pyrenoidosa*. Their results indicated better biocidal properties of the binary mixture of TNPs and TNTs compared to TNTs alone for both types of algae. Additionally, the bactericidal properties of TNTs could be enhanced by the use of antibacterial coatings such as chitosan and silver nanoparticles (Figure 11) [145,146].

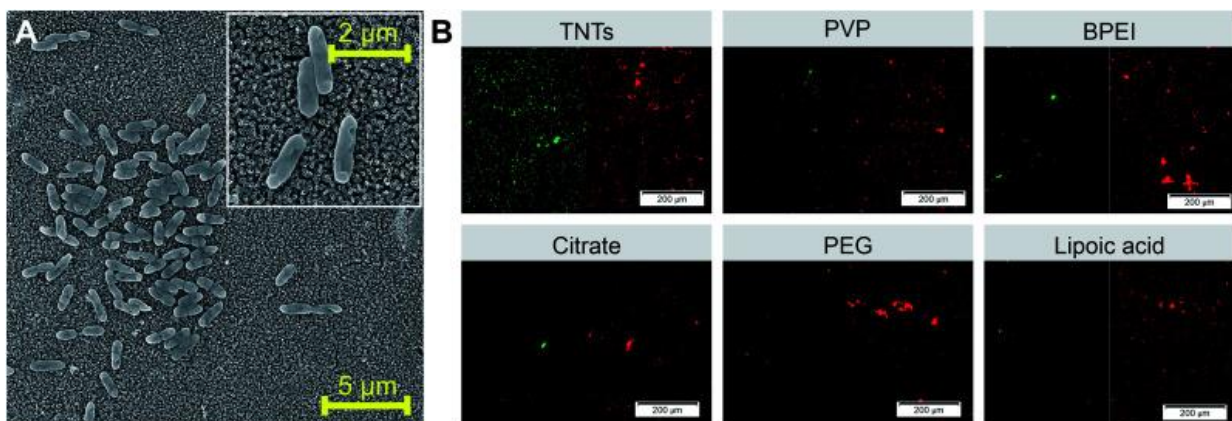


**Figure 11.** (A) SEM images of *P. aeruginosa* adhered on control TNT sample and bacteria shown in detail in the insert of (A). (B) Live/dead fluorescence images of *P. aeruginosa* adhered on differently functionalized Ag-NPs decorated on TNTs (red = dead cells; green = live cells). Abbreviations: polyvinylpyrrolidone, PVP; branched polyethyleneimine, BPEI; polyethylene glycol, PEG. Reproduced from [145].

## 6. Concluding Remarks

In this review, we presented some commonly used techniques for the synthesis and property modification of TNTs. Vertically aligned TNTs can be best modified via the electrochemical anodization method. TNTs have exhibited large potential for application in the energy sector, in water purification, and in the biomedical field. Nanostructured TNTs with controllable length, wall thickness, and pore size provide a large surface area for high-performance solar energy conversion. Drug-eluting deep nanostructures have facilitated interaction with biological molecules and biopolymers, enhancing the prospects of tissue regeneration. Furthermore, photocatalysis induced by TNTs is effective against organic pollutants as well as microorganisms.

Although the synthesis mechanism of TNTs has been greatly explored, we still face the challenge of understanding the effect of various electrolytes and growth parameters. The formation mechanism of TNTs is known; however, a detailed comprehension of electrolyte species and their interaction kinetics with the surface of titanium is of extreme importance because it directly affects the morphology, dimensions, and resulting properties of the TNTs. Once the theory behind the TNT formation is established, the photocatalytic, photovoltaic, and photoelectrochemical performance of solar cells may be enhanced. The mechanism of TNTs' interaction with biological entities may be further explored, and more effective drug delivery systems can be generated. Hence, a coalesced theory to describe the growth of TNTs via various routes is required for further advancement in the subject.

**Author Contributions:** Conceptualization, A.N. and M.A.U.R.; resources, S.A.B., M.S.M. and M.A.J.; data curation, S.A.B., M.S.M. and M.A.U.R.; writing—original draft preparation, S.A.B., M.S.M., M.A.J., A.N. and M.A.U.R.; writing—review and editing, S.A.B. and M.A.U.R.; supervision, A.N.; and M.A.U.R.; funding acquisition, M.A.U.R. All authors have read and agreed to the published version of the manuscript.

**Funding:** This research was funded by Innovative and Collaborative Research Grant Partnerships Grant under Pakistan UK Education Gateway (ICRG-2020) [Reference No: 006326/D/ISB/007/2021].

**Conflicts of Interest:** The authors declare no conflict of interest.

## References

1. Salem, S.S.; Hammad, E.N.; Mohamed, A.A.; El-dougDoug, W. A comprehensive review of nanomaterials: Types, synthesis, characterization, and applications. *Bioint. Res. Appl. Chem.* **2022**, *13*, 41. [[CrossRef](#)]
2. Taniguchi, N. On the basic concept of nanotechnology. In Proceedings of the ICPE, Tokyo, Japan, 26–29 August 1974; pp. 18–23.
3. Mulvaney, P. Nanoscience vs Nanotechnology—Defining the Field. *ACS Nano* **2015**, *9*, 2215–2217. [[CrossRef](#)] [[PubMed](#)]
4. Panda, P.K.; Grigoriev, A.; Mishra, Y.K.; Ahuja, R. Progress in supercapacitors: Roles of two dimensional nanotubular materials. *Nanoscale Adv.* **2020**, *2*, 70–108. [[CrossRef](#)] [[PubMed](#)]
5. Wawrzyniak, J.; Grochowska, K.; Karczewski, J.; Kupracz, P.; Ryl, J.; Dołęga, A.; Siuzdak, K. The geometry of free-standing titania nanotubes as a critical factor controlling their optical and photoelectrochemical performance. *Surf. Coat. Technol.* **2020**, *389*, 125628. [[CrossRef](#)]
6. Suttiponparnit, K.; Jiang, J.; Sahu, M.; Suvachittanont, S.; Charinpanitkul, T.; Biswas, P. Role of surface area, primary particle size, and crystal phase on titanium dioxide nanoparticle dispersion properties. *Nanoscale Res. Lett.* **2011**, *6*, 27. [[CrossRef](#)]
7. Wang, H.; Liang, X.; Wang, J.; Jiao, S.; Xue, D. Multifunctional inorganic nanomaterials for energy applications. *Nanoscale* **2020**, *12*, 14–42. [[CrossRef](#)] [[PubMed](#)]
8. Shen, S.; Chen, J.; Wang, M.; Sheng, X.; Chen, X.; Feng, X.; Mao, S.S. Titanium dioxide nanostructures for photoelectrochemical applications. *Prog. Mater. Sci.* **2018**, *98*, 299–385. [[CrossRef](#)]
9. Dai, L.; Chang, D.W.; Baek, J.; Lu, W. Carbon nanomaterials for advanced energy conversion and storage. *Small* **2012**, *8*, 1122. [[CrossRef](#)]
10. Xue, X.; Ji, W.; Mao, Z.; Mao, H.; Wang, Y.; Wang, X.; Ruan, W.; Zhao, B.; Lombardi, J.R. Raman investigation of nanosized TiO<sub>2</sub>: Effect of crystallite size and quantum confinement. *J. Phys. Chem. C* **2012**, *116*, 8792–8797. [[CrossRef](#)]
11. Maduraiveeran, G.; Sasidharan, M.; Jin, W. Earth-abundant transition metal and metal oxide nanomaterials: Synthesis and electrochemical applications. *Prog. Mater. Sci.* **2019**, *106*, 100574. [[CrossRef](#)]

12. Ali, S.; Granbohm, H.; Lahtinen, J. Titania nanotubes prepared by rapid breakdown anodization for photocatalytic decolorization of organic dyes under UV and natural solar light. *Nanoscale Res. Lett.* **2018**, *13*, 179. [[CrossRef](#)]
13. Absalan, Y.; Gholizadeh, M.; Butusov, L.; Bratchikova, I.; Kopylov, V.; Kovalchukova, O. Titania nanotubes (TNTs) prepared through the complex compound of gallic acid with titanium; examining photocatalytic degradation of the obtained TNTs. *Arab. J. Chem.* **2020**, *13*, 7274–7288. [[CrossRef](#)]
14. Poddar, S.; Bit, A.; Sinha, S.K. A study on influence of anodization on the morphology of titania nanotubes over Ti6Al4V alloy in correlation to hard tissue engineering application. *Mater. Chem. Phys.* **2020**, *254*, 123457. [[CrossRef](#)]
15. Pawlik, A.; Rehman, M.A.U.; Nawaz, Q.; Bastan, F.E.; Sulka, G.D.; Boccaccini, A.R. Fabrication and characterization of electrophoretically deposited chitosan-hydroxyapatite composite coatings on anodic titanium dioxide layers. *Electrochim. Acta* **2019**, *307*, 465–473. [[CrossRef](#)]
16. Mohan, L.; Dennis, C.; Padmapriya, N.; Anandan, C.; Rajendran, N. Effect of electrolyte temperature and anodization time on formation of TiO<sub>2</sub> nanotubes for biomedical applications. *Mater. Today Commun.* **2020**, *23*, 101103. [[CrossRef](#)]
17. Tak, M.; Tomar, H.; Mote, R.G. Synthesis of titanium nanotubes (TNT) and its influence on electrochemical micromachining of titanium. *Procedia CIRP* **2020**, *95*, 803–808. [[CrossRef](#)]
18. Quiroz, H.; Cuenca, A.D. Synthesis of self-organized TiO<sub>2</sub> nanotube arrays: Microstructural, stereoscopic, and topographic studies. *J. Appl. Phys.* **2016**, *120*, 051703. [[CrossRef](#)]
19. Roy, P.; Kim, D.; Lee, K.; Spiecker, E.; Schmuki, P. TiO<sub>2</sub> nanotubes and their application in dye-sensitized solar cells. *Nanoscale* **2010**, *2*, 45–59. [[CrossRef](#)]
20. Lin, K.S.; Lin, Y.G.; Cheng, H.W.; Haung, Y.H. Preparation and characterization of V-Loaded titania nanotubes for adsorption/photocatalysis of basic dye and environmental hormone contaminated wastewaters. *Catal. Today* **2018**, *307*, 119–130. [[CrossRef](#)]
21. Chernozem, R.V.; Surmeneva, M.A.; Ignatov, V.P.; Peltek, O.O.; Goncharenko, A.A.; Muslimov, A.R.; Timin, A.S.; Tyurin, A.I.; Ivanov, Y.F.; Grandini, C.R.; et al. Comprehensive characterization of titania nanotubes fabricated on Ti-Nb alloys: Surface topography, structure, physicochemical behavior, and a cell culture assay. *ACS Biomater. Sci. Eng.* **2020**, *6*, 1487–1499. [[CrossRef](#)]
22. Hasan, A.; Saxena, V.; Pandey, L.M. Surface functionalization of Ti6Al4V via self-assembled monolayers for improved protein adsorption and fibroblast adhesion. *Langmuir* **2018**, *34*, 3494–3506. [[CrossRef](#)] [[PubMed](#)]
23. Li, T.; Gulati, K.; Wang, N.; Zhang, Z.; Ivanovski, S. Understanding and augmenting the stability of therapeutic nanotubes on anodized titanium implants. *Mater. Sci. Eng. C* **2018**, *88*, 182–195. [[CrossRef](#)] [[PubMed](#)]
24. Kunrath, M.F.; Vargas, A.L.M.; Sesterheim, P.; Teixeira, E.R.; Hubler, R. Extension of hydrophilicity stability by reactive plasma treatment and wet storage on TiO<sub>2</sub> nanotube surfaces for biomedical implant applications. *J. R. Soc. Interface* **2020**, *17*, 20200650. [[CrossRef](#)]
25. Mansoorianfar, M.; Khataee, A.; Riahi, Z.; Shahin, K.; Asadnia, M.; Razmjou, A.; Hojjati-Najafabadi, A.; Mei, C.; Orooji, Y.; Li, D. Scalable fabrication of tunable titanium nanotubes via sonoelectrochemical process for biomedical applications. *Ultrason. Sonochem.* **2020**, *64*, 104783. [[CrossRef](#)] [[PubMed](#)]
26. Xu, Y.; Zangari, G. TiO<sub>2</sub> nanotubes architectures for solar energy conversion. *Coatings* **2021**, *11*, 931. [[CrossRef](#)]
27. Alijani, M.; Sopha, H.; Ng, S.; Macak, J.M. High aspect ratio TiO<sub>2</sub> nanotube layers obtained in a very short anodization time. *Electrochim. Acta* **2021**, *376*, 138080. [[CrossRef](#)]
28. Macak, J.M.; Jarosova, M.; Jäger, A.; Sopha, H.; Klementová, M. Influence of the Ti microstructure on anodic self-organized TiO<sub>2</sub> nanotube layers produced in ethylene glycol electrolytes. *Appl. Surf. Sci.* **2016**, *371*, 607–612. [[CrossRef](#)]
29. Li, D.G.; Chen, D.R.; Wang, J.D.; Liang, P. Effect of acid solution, fluoride ions, anodic potential and time on the microstructure and electronic properties of self-ordered TiO<sub>2</sub> nanotube arrays. *Electrochim. Acta* **2016**, *207*, 152–163. [[CrossRef](#)]
30. Abdullah, M.; Kamarudin, S.K. Titanium dioxide nanotubes (TNT) in energy and environmental applications: An overview. *Renew. Sustain. Energy Rev.* **2017**, *76*, 212–225. [[CrossRef](#)]
31. Gulati, K.; Santos, A.; Findlay, D.; Losic, D. Optimizing anodization conditions for the growth of titania nanotubes on curved surfaces. *J. Phys. Chem. C* **2015**, *119*, 16033–16045. [[CrossRef](#)]
32. Çırak, B.B.; Karadeniz, S.M.; Kılınc, T.; Caglar, B.; Ekinci, A.E.; Yelgin, H.; Kürekçi, M. Synthesis, surface properties, crystal structure and dye sensitized solar cell performance of TiO<sub>2</sub> nanotube arrays anodized under different voltages. *Vacuum* **2017**, *144*, 183–189. [[CrossRef](#)]
33. Mansoorianfar, M.; Rahighi, R.; Hojjati-Najafabadi, A.; Mei, C.; Li, D. Amorphous/crystalline phase control of Nanotubular TiO<sub>2</sub> membranes via pressure-engineered anodizing. *Mater. Des.* **2020**, *198*, 109314. [[CrossRef](#)]
34. Nikolai, T.; Larina, L.; Kang, J.K.; Shevaleevskiy, O. Sol-gel processed TiO<sub>2</sub> nanotube photoelectrodes for dye-sensitized solar cells with enhanced photovoltaic performance. *Nanomaterials* **2020**, *10*, 296. [[CrossRef](#)]
35. Owens, G.J.; Singh, R.K.; Foroutan, F.; Alqaysi, M.; Han, C.-M.; Mahapatra, C.; Kim, H.-W.; Knowles, J.C. Sol-gel based materials for biomedical applications. *Prog. Mater. Sci.* **2015**, *77*, 1–79. [[CrossRef](#)]



36. Yue, L.; Gao, W.; Zhang, D.; Guo, F.; Ding, W.; Chen, Y. Colloids Seeded Deposition: Growth of Titania Nanotubes in Solution. *Am. Chem. Soc.* **2006**, *128*, 11042–11043. [[CrossRef](#)]
37. Cossuet, T.; Rapenne, L.; Renou, G.; Appert, E.; Consonni, V. Template-assisted growth of open-ended TiO<sub>2</sub> nanotubes with hexagonal shape using atomic layer deposition. *Cryst. Growth Des.* **2021**, *21*, 125–132. [[CrossRef](#)]
38. Kaur, A.; Bajaj, B.; Kaushik, A.; Saini, A.; Sud, D. A review on template assisted synthesis of multi-functional metal oxide nanostructures: Status and prospects. *Mater Sci. Eng. B* **2022**, *286*, 116005. [[CrossRef](#)]
39. Zavala, M.A.L.; Morales, S.A.L.; Santos, M.Á. Synthesis of stable TiO<sub>2</sub> nanotubes: Effect of hydrothermal treatment, acid washing and annealing temperature. *Heliyon* **2017**, *3*, e00456. [[CrossRef](#)]
40. Mamaghani, A.H.; Haghghat, F.; Lee, C.-S. Hydrothermal/solvothermal synthesis and treatment of TiO<sub>2</sub> for photocatalytic degradation of air pollutants: Preparation, characterization, properties, and performance. *Chemosphere* **2018**, *219*, 804–825. [[CrossRef](#)]
41. Huang, J.; Zhang, K.; Lai, Y. Recent advances in preparation, modification and applications of TiO<sub>2</sub> nanostructures by electrochemical anodization. *Handb. Nanoelectrochem.* **2015**, 1379–1416. [[CrossRef](#)]
42. Giorgi, L.; Dikonimos, T.; Giorgi, R.; Buonocore, F.; Faggio, G.; Messina, G.; Lisi, N. Electrochemical synthesis of self-organized TiO<sub>2</sub> crystalline nanotubes without annealing. *Nanotechnology* **2018**, *29*, 095604. [[CrossRef](#)] [[PubMed](#)]
43. Bavykin, D.V.; Walsh, F.C. Titanate and titania nanotubes synthesis, properties and applications introduction and scope. In *Titanate and Titania Nanotubes: Synthesis, Properties and Applications*; Royal Soc Chemistry: Cambridge, UK, 2010; pp. 1–19.
44. Albu, S.P.; Schmuki, P. Influence of anodization parameters on the expansion factor of TiO<sub>2</sub> nanotubes. *Electrochim. Acta* **2012**, *91*, 90–95. [[CrossRef](#)]
45. Chernozem, R.V.; Surmeneva, M.A.; Surmenev, R.A. Influence of anodization time and voltage on the parameters of TiO<sub>2</sub> nanotubes. *IOP Conf. Ser. Mater. Sci. Eng.* **2016**, *116*, 12025. [[CrossRef](#)]
46. Escada, A.L.; Nakazato, R.Z.; Claro, A.P.R.A. Influence of anodization parameters in the TiO<sub>2</sub> nanotubes formation on Ti-7.5Mo alloy surface for biomedical application. *Mater. Res.* **2017**, *20*, 1282–1290. [[CrossRef](#)]
47. Fu, Y.; Mo, A. A review on the electrochemically self-organized titania nanotube arrays: Synthesis, Modifications, and biomedical applications. *Nanoscale Res. Lett.* **2018**, *13*, 187. [[CrossRef](#)]
48. Lim, Y.-C.; Zainal, Z.; Tan, W.-T.; Hussein, M.Z. Anodization parameters influencing the growth of titania nanotubes and their photoelectrochemical response. *Int. J. Photoenergy* **2012**, *2012*, 638017. [[CrossRef](#)]
49. Shah, U.H.; Rahman, Z.; Deen, K.M.; Asgar, H.; Shabib, I.; Haider, W. Investigation of the formation mechanism of titanium oxide nanotubes and its electrochemical evaluation. *J. Appl. Electrochem.* **2017**, *47*, 1147–1159. [[CrossRef](#)]
50. Ban, T.; Tanaka, Y.; Ohya, Y. Fabrication of titania films by sol-gel method using transparent colloidal aqueous solutions of anatase nanocrystals. *Thin Solid Films* **2010**, *519*, 3468–3474. [[CrossRef](#)]
51. Lee, M.; Kim, T.; Bae, C.; Shin, H.; Kim, J. Fabrication and applications of metal-oxide nano-tubes. *JOM* **2010**, *62*, 44–49. [[CrossRef](#)]
52. Sungur, Å. Titanium Dioxide Nanoparticles. In *Handbook of Nanomaterials and Nanocomposites for Energy and Environmental Applications*; Kharissova, O.V., Martnez, L.M.T., Kharisov, B.I., Eds.; Springer International Publishing: Cham, Switzerland, 2020; pp. 1–18.
53. Karaman, M.; Saripek, F.; Koysuren, O.; Yildiz, H. Template assisted synthesis of photocatalytic titanium dioxide nanotubes by hot filament chemical vapor deposition method. *Appl. Surf. Sci.* **2013**, *283*, 993–998. [[CrossRef](#)]
54. Taziwa, R.; Meyer, E.; Takata, N. Structural and raman spectroscopic characterization of C-TiO<sub>2</sub> Nanotubes synthesized by a template assisted sol-gel technique. *J. Nanosci. Nanotechnol. Res.* **2017**, *1*, 4.
55. Kumar, A.; Yadav, N.; Bhatt, M.; Mishra, N.K.; Chaudhary, P.; Singh, R. Sol-gel derived nanomaterials and it's applications: A review. *Res. J. Chem. Sci.* **2015**, *5*, 1–6.
56. Fu, C.; Hu, X.; Yang, Z.; Shen, L.; Zheng, Z. Preparation and properties of waterborne bio-based polyurethane/siloxane cross-linked films by an in situ sol-gel process. *Prog. Org. Coat.* **2015**, *84*, 18–27. [[CrossRef](#)]
57. Tan, A.W.; -Murphy, B.P.; Ahmad, R.; Akbar, S.A. Review of titania nanotubes: Fabrication and cellular response. *Ceram. Int.* **2012**, *38*, 4421–4435. [[CrossRef](#)]
58. Liu, N.; Albu, S.P.; Lee, K.; So, S.; Schmuki, P. Water annealing and other low temperature treatments of anodic TiO<sub>2</sub> nanotubes: A comparison of properties and efficiencies in dye sensitized solar cells and for water splitting. *Electrochim. Acta* **2012**, *82*, 98–102. [[CrossRef](#)]
59. Ahmad, A.; Haq, E.U.; Akhtar, W.; Arshad, M.; Ahmad, Z. Synthesis and characterization of titania nanotubes by anodizing of titanium in fluoride containing electrolytes. *Appl. Nanosci.* **2017**, *7*, 701–710. [[CrossRef](#)]
60. Gibran, K.; Ibadurrahman, M. Effect of electrolyte type on the morphology and crystallinity of TiO<sub>2</sub> nanotubes from Ti-6Al-4V anodization. *IOP Conf. Ser. Earth Environ. Sci.* **2018**, *105*, 12038. [[CrossRef](#)]
61. Kapusta-Kołodziej, J.; Syrek, K.; Pawlik, A.; Jarosz, M.; Tynkevych, O.; Sulka, G.D. Effects of anodizing potential and temperature on the growth of anodic TiO<sub>2</sub> and its photoelectrochemical properties. *Appl. Surf. Sci.* **2016**, *396*, 1119–1129. [[CrossRef](#)]
62. Jarosz, M.; Pawlik, A.; -Kołodziej, J.K.; Jaskuła, M.; Sulka, G.D. Effect of the previous usage of electrolyte on growth of anodic titanium dioxide (ATO) in a glycerol-based electrolyte. *Electrochim. Acta* **2014**, *136*, 412–421. [[CrossRef](#)]

63. Li, Y.; Ma, Q.; Han, J.; Ji, L.; Wang, J.; Chen, J.; Wang, Y. Controllable preparation, growth mechanism and the properties research of TiO<sub>2</sub> nanotube arrays. *Appl. Surf. Sci.* **2014**, *297*, 103–108. [[CrossRef](#)]
64. Muzakir, M.M.; Zainal, Z.; Lim, H.N.; Abdullah, A.H.; Bahrudin, N.N.; Ali, M.S. Electrochemically reduced titania nanotube synthesized from glycerol-based electrolyte as supercapacitor electrode. *Energies* **2020**, *13*, 2767. [[CrossRef](#)]
65. Srimuangmak, K.; Niyomwas, S. Effects of voltage and addition of water on photocatalytic activity of TiO<sub>2</sub> nanotubes prepared by anodization method. *Energy Procedia* **2011**, *9*, 435–439. [[CrossRef](#)]
66. Shah, U.H.; Deen, K.M.; Asgar, H.; Rahman, Z.; Haider, W. Understanding the mechanism of TiO<sub>2</sub> nanotubes formation at low potentials (at % 8V) through electrochemical methods. *J. Electroanal. Chem.* **2017**, *807*, 228–234. [[CrossRef](#)]
67. Ono, S.; Asoh, H. A new perspective on pore growth in anodic alumina films. *Electrochem. Commun.* **2021**, *124*, 106972. [[CrossRef](#)]
68. Riboni, F.; Nguyen, N.T.; So, S.; Schmuki, P. Aligned metal oxide nanotube arrays: Key-aspects of anodic TiO<sub>2</sub> nanotube formation and properties. *Nanoscale Horiz.* **2016**, *1*, 445–466. [[CrossRef](#)]
69. Tesler, A.B.; Altomare, M.; Schmuki, P. Morphology and optical properties of highly ordered TiO<sub>2</sub> nanotubes grown in NH<sub>4</sub>F/o-H<sub>3</sub>PO<sub>4</sub> electrolytes in view of light-harvesting and catalytic applications. *ACS Appl. Nano Mater.* **2020**, *3*, 10646–10658. [[CrossRef](#)]
70. Li, J. Hydrodynamic control of titania nanotube formation on Ti-6Al-4V alloys enhances osteogenic differentiation of human mesenchymal stromal cells. *Mater. Sci. Eng. C* **2020**, *109*, 110562. [[CrossRef](#)]
71. Pasikhani, J.V.; Gilani, N.; Pirbazari, A.E. The effect of the anodization voltage on the geometrical characteristics and photocatalytic activity of TiO<sub>2</sub> nanotube arrays. *Nano Struct. Nano Objects* **2016**, *8*, 7–14. [[CrossRef](#)]
72. Cortes, F.J.Q.; Arias-Monje, P.J.; Phillips, J.; Zea, H. Empirical kinetics for the growth of titania nanotube arrays by potentiostatic anodization in ethylene glycol. *Mater. Des.* **2016**, *96*, 80–89. [[CrossRef](#)]
73. Joanna, K.-K.; Syrek, K.; Sulka, G.D. Synthesis and photoelectrochemical properties of anodic oxide films on titanium formed by pulse anodization. *J. Electrochem. Soc.* **2018**, *165*, H838. [[CrossRef](#)]
74. Regonini, D.; Clemens, F. Anodized TiO<sub>2</sub> nanotubes: Effect of anodizing time on film length, morphology and photoelectrochemical properties. *Mater. Lett.* **2014**, *142*, 97–101. [[CrossRef](#)]
75. Joanna, K.-K.; Chudecka, A.; Sulka, G.D. 3D nanoporous titania formed by anodization as a promising photoelectrode material. *J. Electroanal. Chem.* **2018**, *823*, 221–233. [[CrossRef](#)]
76. Sturgeon, M.R.; Lai, P.; Hu, M.Z. A comparative study of anodized titania nanotube architectures in aqueous and nonaqueous solutions. *J. Mater. Res.* **2011**, *26*, 2612–2623. [[CrossRef](#)]
77. Mahmoud, M. Self-ordered TiO<sub>2</sub> nanotubes prepared by anodization in fluorine-free electrolyte as additive-free anode for lithium-ion microbatteries. *ECS Meet. Abstr.* **2019**, *MA2019-04*, 76. [[CrossRef](#)]
78. Shuai, Q. A novel elaboration for various morphologies of three-layer TiO<sub>2</sub> nanotubes by oxygen bubble mould. *Mater. Res. Bull.* **2018**, *106*, 220–227. [[CrossRef](#)]
79. Dussan, A.; Boharrquez, A.; Quiroz, H.P. Effect of annealing process in TiO<sub>2</sub> thin films: Structural, morphological, and optical properties. *Appl. Surf. Sci.* **2017**, *424*, 111–114. [[CrossRef](#)]
80. Das, S.; Zazpe, R.; Prikryl, J.; Knotek, P.; Krbal, M.; Sopha, H.; Podzemna, V.; Macak, J.M. Influence of annealing temperatures on the properties of low aspect-ratio TiO<sub>2</sub> nanotube layers. *Electrochim. Acta* **2016**, *213*, 452–459. [[CrossRef](#)]
81. Bauer, S.; Pittrof, A.; Tsuchiya, H.; Schmuki, P. Size-effects in TiO<sub>2</sub> nanotubes: Diameter dependent anatase/rutile stabilization. *Electrochem. Commun.* **2011**, *13*, 538–541. [[CrossRef](#)]
82. Aiempnanakit, M.; Lumpol, V.; Mangsup, T.; Triamnak, N.; Sritharathikun, J.; Suwanchawalit, C. Fabrication of titanium dioxide nanotubes and their photovoltaic performance for dye-sensitized solar cells. *Int. J. Electrochem. Sci.* **2020**, *15*, 10392–10405. [[CrossRef](#)]
83. Bai, Y.; Mora-Seró, I.; de Angelis, F.; Bisquert, J.; Wang, P. Titanium dioxide nanomaterials for photovoltaic applications. *Chem. Rev.* **2014**, *114*, 10095–10130. [[CrossRef](#)]
84. Venkatachalam, P.; Joby, N.G.; Krishnakumar, N. Enhanced photovoltaic characterization and charge transport of TiO<sub>2</sub> nanoparticles/nanotubes composite photoanode based on indigo carmine dye-sensitized solar cells. *J. Sol-Gel Sci. Technol.* **2013**, *67*, 618–628. [[CrossRef](#)]
85. Qadir, M.B.; Li, Y.; Sahito, I.A.; Arbab, A.A.; Sun, K.C.; Mengal, N.; Memon, A.A.; Jeong, S.H. Highly functional TNTs with superb photocatalytic, optical, and electronic performance achieving record PV efficiency of 10.1% for 1D-based DSSCs. *Small* **2016**, *12*, 4508–4520. [[CrossRef](#)] [[PubMed](#)]
86. Haran, N.H.; Yousif, Q.A. The efficiency of TiO<sub>2</sub> nanotube photoanode with graphene nanoplatelets as counter electrode for a dye-sensitized solar cell. *Int. J. Ambient Energy* **2022**, *43*, 336–343. [[CrossRef](#)]
87. Mathew, A.; Rao, G.M.; Munichandraiah, N. Effect of TiO<sub>2</sub> electrode thickness on photovoltaic properties of dye sensitized solar cell based on randomly oriented Titania nanotubes. *Mater. Chem. Phys.* **2011**, *127*, 95–101. [[CrossRef](#)]
88. Li, F.; Chen, C.; Tan, F.; Yue, G.; Shen, L.; Zhang, W. A new method to disperse CdS quantum dot-sensitized TiO<sub>2</sub> nanotube arrays into P3HT:PCBM layer for the improvement of efficiency of inverted polymer solar cells. *Nanoscale Res. Lett.* **2014**, *9*, 240. [[CrossRef](#)]
89. Kumar, S.; Vats, T.; Sharma, S.N.; Kumar, J. Investigation of annealing effects on TiO<sub>2</sub> nanotubes synthesized by a hydrothermal method for hybrid solar cells. *Optik* **2018**, *171*, 492–500. [[CrossRef](#)]

90. Lee, J.; Jho, J.Y. Fabrication of highly ordered and vertically oriented TiO<sub>2</sub> nanotube arrays for ordered heterojunction polymer/inorganic hybrid solar cell. *Sol. Energy Mater. Sol. Cells* **2011**, *95*, 3152–3156. [[CrossRef](#)]
91. Javed, H.M.A.; Ahmad, M.I.; Que, W.; Qureshi, A.A.; Sarfaraz, M.; Hussain, S.; Iqbal, M.Z.; Nisar, M.Z.; Shahid, M.; AlGarni, T.S. Encapsulation of TiO<sub>2</sub> nanotubes with Cs nanoparticles to enhance electron injection and thermal stability of perovskite solar cells. *Surf. Interfaces* **2021**, *23*, 101033. [[CrossRef](#)]
92. Zhang, J.; Gao, X.; Deng, Y.; Li, B.; Yuan, C. Life cycle assessment of titania perovskite solar cell technology for sustainable design and manufacturing. *ChemSusChem* **2015**, *8*, 3882–3891. [[CrossRef](#)]
93. Wang, X.; A Kulkarni, S.; Li, Z.; Xu, W.; Batabyal, S.K.; Zhang, S.; Cao, A.; Wong, L.H. Wire-shaped perovskite solar cell based on TiO<sub>2</sub> nanotubes. *Nanotechnology* **2016**, *27*, 20LT01. [[CrossRef](#)]
94. Husain, A.A.F. A review of transparent solar photovoltaic technologies. *Renew. Sustain. Energy Rev.* **2018**, *94*, 779–791. [[CrossRef](#)]
95. Zhang, M.; Chen, T.; Wang, Y. Insights into TiO<sub>2</sub> polymorphs: Highly selective synthesis, phase transition, and their polymorph-dependent properties. *RSC Adv.* **2017**, *7*, 52755–52761. [[CrossRef](#)]
96. Barbieriková, Z.; Plížingrová, E.; Motlochová, M.; Bezdička, P.; Boháček, J.; Dvoranová, D.; Brezová, V. N-Doped titanium dioxide nanosheets: Preparation, characterization and UV/visible-light activity. *Appl. Catal. B Environ.* **2018**, *232*, 397–408. [[CrossRef](#)]
97. Dambournet, D.; Belharouak, I.; Amine, K. Tailored preparation methods of TiO<sub>2</sub> anatase, rutile, brookite: Mechanism of formation and electrochemical properties. *Chem. Mater.* **2010**, *22*, 1173–1179. [[CrossRef](#)]
98. Mansfeldova, V.; Zlamalova, M.; Tarabkova, H.; Janda, P.; Vorokhta, M.; Piliat, L.; Kavan, L. Work function of TiO<sub>2</sub> (anatase, rutile, and brookite) single crystals: Effects of the environment. *J. Phys. Chem. C* **2021**, *125*, 1902–1912. [[CrossRef](#)]
99. Hou, X.; Aitola, K.; Lund, P.D. TiO<sub>2</sub> nanotubes for dye-sensitized solar cells—A review. *Energy Sci. Eng.* **2021**, *9*, 921–937. [[CrossRef](#)]
100. Jen, H.-P.; Lin, M.-H.; Li, L.-L.; Wu, H.-P.; Huang, W.-K.; Cheng, P.-J.; Diau, E.W.-G. High-performance large-scale flexible dye-sensitized solar cells based on anodic TiO<sub>2</sub> nanotube arrays. *ACS Appl. Mater. Interfaces* **2013**, *5*, 10098–10104. [[CrossRef](#)]
101. Wang, M.; Bai, J.; Le Formal, F.; Moon, S.-J.; Cevey-Ha, L.; Humphry-Baker, R.; Grätzel, C.; Zakeeruddin, S.M.; Grätzel, M. Solid-state dye-sensitized solar cells using ordered TiO<sub>2</sub> nanorods on transparent conductive oxide as photoanodes. *J. Phys. Chem. C* **2012**, *116*, 3266–3273. [[CrossRef](#)]
102. Subramaniam, M.R.; Kumaresan, D.; Jothi, S.; McGettrick, J.D.; Watson, T.M. Reduced graphene oxide wrapped hierarchical TiO<sub>2</sub> nanorod composites for improved charge collection efficiency and carrier lifetime in dye sensitized solar cells. *Appl. Surf. Sci.* **2018**, *428*, 439–447. [[CrossRef](#)]
103. Liao, J.-Y.; Lei, B.-X.; Chen, H.-Y.; Kuang, D.-B.; Su, C.-Y. Oriented hierarchical single crystalline anatase TiO<sub>2</sub> nanowire arrays on Ti-foil substrate for efficient flexible dye-sensitized solar cells. *Energy Environ. Sci.* **2012**, *5*, 5750–5757. [[CrossRef](#)]
104. Debnath, K.; Majumder, T.; Mondal, S.P. Photoelectrochemical study of hydrothermally grown vertically aligned rutile TiO<sub>2</sub> nanorods. *Chem. Phys.* **2022**, *561*, 111609. [[CrossRef](#)]
105. Sugathan, V.; John, E.; Sudhakar, K. Recent improvements in dye sensitized solar cells: A review. *Renew. Sustain. Energy Rev.* **2015**, *52*, 54–64. [[CrossRef](#)]
106. Bagher, A.M. Types of solar cells and application. *Am. J. Opt. Photonics* **2015**, *3*, 94. [[CrossRef](#)]
107. Sharma, S.; Jain, K.K.; Sharma, A. Solar cells: In research and applications—A review. *Mater. Sci. Appl.* **2015**, *6*, 1145–1155. [[CrossRef](#)]
108. Karthick, S.; Hemalatha, K.; Balasingam, S.K.; Clinton, F.M.; Akshaya, S.; Kim, H. Dye-Sensitized Solar Cells: History, Components, Configuration, and Working Principle. In *Interfacial Engineering in Functional Materials for Dye-Sensitized Solar Cells*; John Wiley & Sons: Hoboken, NJ, USA, 2016; pp. 1–16. [[CrossRef](#)]
109. Ma, C.; Hou, D.; Jiang, J.; Fan, Y.; Li, X.; Li, T.; Ma, Z.; Ben, H.; Xiong, H. Elucidating the synergic effect in nanoscale MoS<sub>2</sub>/TiO<sub>2</sub> heterointerface for Na-Ion storage. *Adv. Sci.* **2022**, 2204837. [[CrossRef](#)]
110. Luo, D.; Liu, B.; Fujishima, A.; Nakata, K. TiO<sub>2</sub> nanotube arrays formed on Ti meshes with periodically arranged holes for flexible dye-sensitized solar cells. *ACS Appl. Nano Mater.* **2019**, *2*, 3943–3950. [[CrossRef](#)]
111. Sasidharan, S.; Pradhan, S.C.; Jagadeesh, A.; Nair, B.N.; Mohamed, A.A.; KN, N.U.; Soman, S.; Hareesh, U.N. Bifacial dye-sensitized solar cells with enhanced light scattering and improved power conversion efficiency under full sun and indoor light conditions. *ACS Appl. Energy Mater.* **2020**, *3*, 12584–12595. [[CrossRef](#)]
112. Xu, T.; Qiao, Q. Conjugated polymer–inorganic semiconductor hybrid solar cells. *Energy Environ. Sci.* **2011**, *4*, 2700–2720. [[CrossRef](#)]
113. Heo, J.H.; Im, K.; Kim, J.; Im, S.H. Efficient metal halide perovskite solar cells prepared by reproducible electrospray coating on vertically aligned TiO<sub>2</sub> nanorod electrodes. *ACS Appl. Mater. Interfaces* **2019**, *12*, 886–892. [[CrossRef](#)]
114. Hsu, S.-C.; Liao, W.-P.; Lin, W.-H.; Wu, J.-J. Modulation of photocarrier dynamics in indoline dye-modified TiO<sub>2</sub> nanorod Array/P3HT hybrid solar cell with 4-tert-Butylpyridine. *J. Phys. Chem. C* **2012**, *116*, 25721–25726. [[CrossRef](#)]
115. Chatterjee, S.; Patra, W.S.; Rout, B.; Glass, G.A.; D’Souza, F.; Chatterjee, S. Achievement of superior efficiency of TiO<sub>2</sub> nanorod-nanoparticle composite photoanode in dye sensitized solar cell. *J. Alloys Compd.* **2020**, *826*, 154188. [[CrossRef](#)]
116. Cheng, Y.; Yang, H.; Yang, Y.; Huang, J.; Wu, K.; Chen, Z.; Wang, X.; Lin, C.; Lai, Y. Progress in TiO<sub>2</sub> nanotube coatings for biomedical applications: A review. *J. Mater. Chem. B* **2018**, *6*, 1862–1886. [[CrossRef](#)] [[PubMed](#)]



117. Li, Y.; Yang, Y.; Li, R.; Tang, X.; Guo, D.; Qing, Y.; Qin, Y. Enhanced antibacterial properties of orthopedic implants by titanium nanotube surface modification: A review of current techniques. *Int. J. Nanomed.* **2019**, *14*, 7217–7236. [[CrossRef](#)] [[PubMed](#)]
118. Gai, X.; Bai, Y.; Li, S.; Hou, W.; Hao, Y.; Zhang, X.; Yang, R.; Misra, R. In-situ monitoring of the electrochemical behavior of cellular structured biomedical Ti-6Al-4V alloy fabricated by electron beam melting in simulated physiological fluid. *Acta Biomater.* **2020**, *106*, 387–395. [[CrossRef](#)]
119. Mahyad, B. Biomedical applications of TiO<sub>2</sub> nanostructures: Recent Advances. *Int. J. Nanomed.* **2020**, *15*, 3447–3470.
120. Souza, J.C.M.; Sordi, M.B.; Kanazawa, M.; Ravindran, S.; Henriques, B.; Silva, F.S.; Aparicio, C.; Cooper, L.F. Nano-scale modification of titanium implant surfaces to enhance osseointegration. *Acta Biomater.* **2019**, *94*, 112–131. [[CrossRef](#)]
121. Kaur, M.; Singh, K. Review on titanium and titanium based alloys as biomaterials for orthopaedic applications. *Mater. Sci. Eng. C* **2019**, *102*, 844–862. [[CrossRef](#)]
122. Hu, N.; Wu, Y.; Xie, L.; Yusuf, S.M.; Gao, N.; Starink, M.J.; Tong, L.; Chu, P.K.; Wang, H. Enhanced interfacial adhesion and osseointegration of anodic TiO<sub>2</sub> nanotube arrays on ultra-fine-grained titanium and underlying mechanisms. *Acta Biomater.* **2020**, *106*, 360–375. [[CrossRef](#)]
123. Abbass, M.K.; Khadhim, M.J.; Jasim, A.N.; Issa, M.J. A study the effect of porosity of bio-active ceramic hydroxyapatite coated by electrophoretic deposition on the Ti6Al4V alloy substrate. *J. Phys. Conf. Ser.* **2021**, *1773*, 012035. [[CrossRef](#)]
124. Esmaeilnejad, A.; Mahmoudi, P.; Zamanian, A.; Mozafari, M. Synthesis of titanium oxide nanotubes and their decoration by MnO nanoparticles for biomedical applications. *Ceram. Int.* **2019**, *45*, 19275–19282. [[CrossRef](#)]
125. Kunrath, M.F.; Penha, N.; Ng, J.C. Anodization as a promising surface treatment for drug delivery implants and a non-cytotoxic process for surface alteration: A pilot study. *J. Osseointegration* **2020**, *12*, 45–49. [[CrossRef](#)]
126. López-Pavón, L.; Dagnino-Acosta, D.; López-Cuellar, E.; Meléndez-Anzures, F.; Zárate-Triviño, D.; Barrón-González, M.; Moreno-Cortez, I.; Kim, H.Y.; Miyazaki, S. Synthesis of nanotubular oxide on Ti-24Zr-10Nb-2Sn as a drug-releasing system to prevent the growth of *Staphylococcus aureus*. *Chem. Pap.* **2021**, *75*, 2441–2450. [[CrossRef](#)]
127. Effendy, W.N.F.W.E.; Mydin, R.B.S.; Gazzali, A.M.; Sreekantan, S. Therapeutic nano-device: Study of biopolymer coating on titania nanotubes array loaded with chemodrug targeted for localized cancer therapy application. *IOP Conf. Ser. Mater. Sci. Eng.* **2020**, *932*, 012116. [[CrossRef](#)]
128. Kwiatkowski, S.; Knap, B.; Przystupski, D.; Saczko, J.; Kędzierska, E.; Knap-Czop, K.; Kotlińska, J.; Michel, O.; Kotowski, K.; Kulbacka, J. Photodynamic therapy—Mechanisms, photosensitizers and combinations. *Biomed. Pharmacother.* **2018**, *106*, 1098–1107. [[CrossRef](#)] [[PubMed](#)]
129. Meng, Z.; Xue, H.; Wang, T.; Chen, B.; Dong, X.; Yang, L.; Dai, J.; Lou, X.; Xia, F. Aggregation-induced emission photosensitizer-based photodynamic therapy in cancer: From chemical to clinical. *J. Nanobiotechnol.* **2022**, *20*, 344. [[CrossRef](#)]
130. Jiménez, V.A.; Moreno, N.; Guzmán, L.; Torres, C.C.; Campos, C.H.; Alderete, J.B. Visible-light-responsive folate-conjugated titania and alumina nanotubes for photodynamic therapy applications. *J. Mater. Sci.* **2020**, *55*, 6976–6991. [[CrossRef](#)]
131. Qin, J.; Yang, D.; Maher, S.; Lima-Marques, L.; Zhou, Y.; Chen, Y.; Atkins, G.J.; Losic, D. Micro- and nano-structured 3D printed titanium implants with a hydroxyapatite coating for improved osseointegration. *J. Mater. Chem. B* **2018**, *6*, 3136–3144. [[CrossRef](#)]
132. Somsanith, N.; Kim, Y.-K.; Jang, Y.-S.; Lee, Y.-H.; Yi, H.-K.; Jang, J.-H.; Kim, K.-A.; Bae, T.-S.; Lee, M.-H. Enhancing of osseointegration with propolis-loaded TiO<sub>2</sub> nanotubes in rat mandible for dental implants. *Materials* **2018**, *11*, 61. [[CrossRef](#)]
133. Roguska, A.; Belcarz, A.; Zalewska, J.; Hołdyński, M.; Andrzejczuk, M.; Pisarek, M.; Ginalska, G. Metal TiO<sub>2</sub> nanotube layers for the treatment of dental implant infections. *ACS Appl. Mater. Interfaces* **2018**, *10*, 17089–17099. [[CrossRef](#)]
134. Wang, C.; Wang, X.; Lu, R.; Gao, S.; Ling, Y.; Chen, S. Responses of human gingival fibroblasts to superhydrophilic hydrogenated titanium dioxide nanotubes. *Colloids Surf. B Biointerfaces* **2020**, *198*, 111489. [[CrossRef](#)]
135. Wang, C.; Wang, X.; Lu, R.; Gao, S.; Ling, Y.; Chen, S. TiO<sub>2</sub> nanotubes modified with Au nanoparticles for visible-light enhanced antibacterial and anti-inflammatory capabilities. *J. Electroanal. Chem.* **2019**, *842*, 66–73. [[CrossRef](#)]
136. Bandyopadhyay, A.; Shivaram, A.; Mitra, I.; Bose, S. Electrically polarized TiO<sub>2</sub> nanotubes on Ti implants to enhance early-stage osseointegration. *Acta Biomater.* **2019**, *96*, 686–693. [[CrossRef](#)]
137. Dong, Y.; Ye, H.; Liu, Y.; Xu, L.; Wu, Z.; Hu, X.; Ma, J.; Pathak, J.L.; Liu, J.; Wu, G. pH dependent silver nanoparticles releasing titanium implant: A novel therapeutic approach to control peri-implant infection. *Colloids Surf. B Biointerfaces* **2017**, *158*, 127–136. [[CrossRef](#)] [[PubMed](#)]
138. Sasireka, A.; Rajendran, R.; Raj, V. In vitro corrosion resistance and cytocompatibility of minerals substituted apatite/biopolymers duplex coatings on anodized Ti for orthopedic implant applications. *Arab. J. Chem.* **2020**, *13*, 6312–6326. [[CrossRef](#)]
139. Feng, W.; Liu, N.; Gao, L.; Zhou, Q.; Yu, L.; Ye, X.; Huo, J.; Huang, X.; Li, P.; Huang, W. Rapid inactivation of multidrug-resistant bacteria and enhancement of osteoinduction via titania nanotubes grafted with polyguanidines. *J. Mater. Sci. Technol.* **2021**, *69*, 188–199. [[CrossRef](#)]
140. Nezhad, E.Z.; Qu, X.; Musharavati, F.; Jaber, F.; Appleford, M.R.; Bae, S.; Uzun, K.; Struthers, M.; Chowdhury, M.E.; Khandakar, A. Effects of titanium and carbon nanotubes on nano/micromechanical properties of HA/TNT/CNT nanocomposites. *Appl. Surf. Sci.* **2021**, *538*, 148123. [[CrossRef](#)]
141. Tong, T.; Shereef, A.; Wu, J.; Binh, C.T.T.; Kelly, J.J.; Gaillard, J.; Gray, K.A. Effects of Material morphology on the phototoxicity of nano-TiO<sub>2</sub> to bacteria. *Environ. Sci. Technol.* **2013**, *47*, 12486–12495. [[CrossRef](#)]



142. Xie, Y.; Fu, D. Photoelectrocatalysis reactivity of independent titania nanotubes. *J. Appl. Electrochem.* **2010**, *40*, 1281–1291. [[CrossRef](#)]
143. Sriram, S.; Nambi, I.M.; Chetty, R. Electrochemical reduction of hexavalent chromium on titania nanotubes with urea as an anolyte additive. *Electrochim. Acta* **2018**, *284*, 427–435. [[CrossRef](#)]
144. Zhuang, W.; Jin, S.; Zhang, F.; Wang, D. Combined toxicity of TiO<sub>2</sub> nanospherical particles and TiO<sub>2</sub> nanotubes to two microalgae with different morphology. *Nanomaterials* **2020**, *10*, 2559. [[CrossRef](#)]
145. Bilek, O.; Fialova, T.; Otahal, A.; Adam, V.; Smerkova, K.; Fohlerova, Z. Antibacterial activity of AgNPs-TiO<sub>2</sub> nanotubes: Influence of different nanoparticle stabilizers. *RSC Adv.* **2020**, *10*, 44601–44610. [[CrossRef](#)] [[PubMed](#)]
146. Pesode, P.A.; Barve, S.B. Recent advances on the antibacterial coating on titanium implant by micro-Arc oxidation process. *Mater. Today Proc.* **2021**, *47*, 5652–5662. [[CrossRef](#)]